

A Flexible Design for Active Reconfigurable Intelligent Surface—A Sub-Array Architecture

Yanze Zhu, Yang Liu, Ming Li, Qingqing Wu, and Qingjiang Shi

Abstract—The emerging reconfigurable intelligent surface (RIS) technology has nowadays been cast with great attentions. The latest research has unveiled that the severe double-fading effect significantly restricts the coverage of pure passive RIS. In this context, a novel active RIS architecture has recently been proposed, where active components are employed to magnify incident signals. Although the active RIS can effectively combat the double-fading loss, one potential drawback is the active components also bring non-negligible energy expenditure. To overcome this shortcoming, we propose a novel sub-array-based RIS construction, which partitions the entire intelligent surface into multiple sub-arrays with each sub-array being flexibly switched on/off. This new architecture entitles one to wisely deactivate the sub-arrays with poor channel fading gains to save energy. Mathematically, the joint sub-array activation and beamforming design towards power consumption and energy efficiency (EE) optimization is highly challenging due to its combinatorial nature. To resolve this challenge, we combine the group sparsity inducing method and the majorization-minimization (MM) framework to develop efficient solutions. Numerical results demonstrate that our proposed solutions can achieve nearly identical performance with the exhaustive-search methods, but with a much lower complexity. Besides, our proposed sub-array-based RIS architecture can significantly improve the power and EE performance.

Index Terms—Active reconfigurable intelligent surface (RIS), power minimization, energy efficiency (EE), beamforming.

I. INTRODUCTION

A. Background

Within the past two years, the world has already launched new research exploring novel technologies and applications

© 2015 IEEE. Personal use of this material is permitted. However, permission to use this material for any other purposes must be obtained from the IEEE by sending a request to pubs-permissions@ieee.org.

Manuscript received 7 December 2022; revised 12 Febrary 2023; accepted 10 April 2023. The work of Yang Liu is supported in part by Grant No. DUT20RC(3)029 and the Open Research Project Programme of the State Key Laboratory of Internet of Things for Smart City (University of Macau) (Ref. No.: SKL-IoTSC(UM)-2021-2023/ORP/GA01/2022). The work of Ming Li is supported in part by the NSFC (Grant No. 61971088), in part by the Fundamental Research Funds for the Central Universities (Grant No. DUT20GJ214), in part by the Natural Science Foundation of Liaoning Province (Grant No. 2020-MS108), and in part by the Open Research Fund of National Mobile Communications Research Laboratory, Southeast University (Grant No. 2021D08). The work of Qingqing Wu is supported by in part by the FDCT under Grant 0119/2020/A3 and Grant 0108/2020/A, and in part by the GDST under Grant 2021A1515011900 and Grant 2020B1212030003. The work of Qingjiang Shi is supported by the NSFC under Grant 62231019. The associate editor coordinating the review of this article and approving it for publication was Dr. L. Song. (*Corresponding author: Yang Liu*)

Y. Zhu, Y. Liu, and M. Li are with the School of Information and Communication Engineering, Dalian University of Technology, Dalian, China, email: 5476z4969y5283z@mail.dlut.edu.cn, yangliu_613@dlut.edu.cn, mli@dlut.edu.cn.

Q. Wu is with the Department of Electronic Engineering, Shanghai Jiao Tong University, 200240, China, email: qingqingwu@sjtu.edu.cn.

Q. Shi is with the School of Software Engineering, Tongji University, Shanghai, China, and also with the Shenzhen Research Institute of Big Data, Shenzhen, China, email: shiqj@tongji.edu.cn.

for the next generation of wireless communication systems [1]. Recently, an emerging technology called reconfigurable intelligent surface (RIS) [2], which is also widely known as intelligent reflecting surface (IRS) [3], has captured great attention from both academia and industry. RIS is a surface consisting of a large number of (passive) reflecting elements that can reflect and adjust the incident electromagnetic waves. Via delicately modifying the phase shifts of reflecting elements, the RIS can reshape the beams of the propagating signals beneficially, which is commonly known as the “passive” beamforming gain. Moreover, the RIS is distinguished by its high energy efficiency (EE) and low hardware cost, since no radio-frequency (RF) circuits are equipped. Due to the above advantages, RIS has recently been visioned as a viable solution to enhance the future wireless communication networks, and its potentials have been extensively explored in many emerging applications [4]-[10]. For instance, it has been verified in [4] that the RIS can significantly improve the transmission rate at the cell edge. The authors of [5] unveiled that the RIS can effectively reduce transmit radio power (TRP) and achieve a power scaling law of N^2 (N is the number of RIS elements). The work [6] considered EE maximization and demonstrated that the system's EE performance can be greatly boosted via deploying the RIS. The promotion of wireless power harvesting in a simultaneously wireless information and power transfer (SWIPT) system with the assistance of the RIS was verified in [7]. Besides, it has been demonstrated that the RIS can significantly boost various system performances in orthogonal frequency division multiplexing (OFDM) scenarios [8], non-orthogonal multiple access (NOMA) systems [9], internet of things (IoT) networks [10] and so on.

Despite its versatility as explored by the existing literature, recently, researchers have come to realize that the passive RIS has some intrinsic drawbacks. As unveiled by [11], the reflected signal from the RIS suffers the “double fading” effect. In fact, the multiplicative fading due to the cascaded channels by way of RIS can be several orders of multitude smaller than that of the direct signal from the transmitter, which severely degrades the beamforming gain of the RIS. Besides, as uncovered by [12] recently, to achieve comparable performance with the classical relay-aided system in practice, the passive RIS requires a prohibitively large number of elements.

To overcome the aforementioned shortcomings, the design of active RIS has been recently proposed in the latest literature [13], [14]. In contrast to the conventional passive RIS that purely reflects incoming signals, active RIS employs amplifiers to magnify the incident signals, which effectively compensates the double fading loss. The advantages of active RIS have been verified by several emerging works [13], [15]-[19]. For

instance, the authors of [13] firstly came up with the structure of active RIS and investigated its capacity. As reported in [13], the active RIS exhibits 129% gain compared to the no-RIS system, in contrast to the negligible 3% gain obtained by the pure passive RIS. The impact of the location of the active RIS was studied in [15], which verified that the active RIS can significantly overcome the “double fading” effect. The authors of [16] studied the active RIS with element-wise power constraints and demonstrated that signal-to-noise-ratio (SNR) can be greatly improved in a single user system. Lately, the work [17] proposed a novel hybrid reflection modulation scheme utilizing both active and passive elements. The authors of [17] analyzed the new design’s performance and illustrated that the introduction of the active elements can effectively improve EE. Besides, the works [18], [19] have also demonstrated that the active RIS can dramatically enhance the spectral efficiency (SE) and EE of the network.

It’s worth noting that, the active RIS outperforms its passive counterpart at the expense of additional energy and hardware expenditure. To further lower the active RIS’ cost, several new designs are recently proposed. For instance, the authors of [18] put forward a new structure where multiple phase-shifters are driven by one single amplifier. This design can effectively reduce the number of amplifiers. The work [19] proposed to deploy two passive RISs between which an amplifier is adopted.

B. Motivation

As previously discussed, the active RIS introduces additional power expenditure. Its non-transmit power consumption mainly comes from phase-shifters and reflection amplifiers. Depending on implementation techniques, phase shifters’ power consumption P_{PS} varies from tens of μW to 10mW [16], [18], [20]-[22] and that of amplifiers, i.e., P_A , ranges from tens of μW to hundreds of mW [16], [18]. Therefore, reasonable average power consumption per RIS element $P_{c,RIS} \triangleq P_{PS} + P_A$ varies from 2mW to 10mW. If we take $P_{c,RIS} = 5\text{mW}$ as an estimate, then the non-transmit power of an active-RIS device with 300 elements can reach up to 1.5W, which is actually comparable to that of an access point (AP). For instance, the small-cell AP device AP1050DN-S by Huawei Technology Ltd. [23] has a maximal power consumption of 8.1W and an average power within 5W. This inspection motivates us to restrict the number of switched-on active RIS elements for power saving.

One feasible solution to make wiser use of energy is to perform “finer” control of the RIS elements—we switch on elements on demand. This can be realized via flexible connection configuration in circuitry. For instance, the works [24]-[32] propose to configure the connection patterns of RF-chains in millimeter wave (mmWave) hybrid precoder to improve beamforming gain while restricting the number of RF-chains for power saving. Specifically, the authors in [24]-[27], [29], [31] propose to dynamically adjust the connection patterns between RF-chains and phase-shifters while the works [28], [30], [32] study fixed connection patterns. Besides, the latest works [18], [20], [33] have proposed sub-array structures to realize block-wise control of the RIS devices. Inspired by these works, we propose a sub-array architecture for active-RIS as shown in Fig. 1, where each sub-array can be flexibly switched on/off as needed.

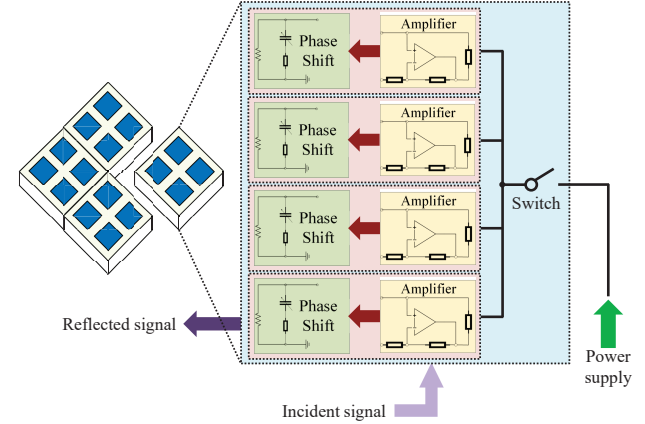


Fig. 1. Proposed sub-array based active RIS structure.

Based on the above proposed switchable sub-array architecture, we are able to jointly optimize sub-array activation control and beamforming design of the RIS device to improve the power consumption and energy efficiency (EE), both of which are critical performance metrics for wireless communications. On the one hand, turning on more elements can effectively increase the dimension of the reflecting array and therefore boost beamforming gain. On the other hand, more activated reflecting elements will induce higher power consumption. This implies we need to strike a balance between the beamforming gain and power consumption when activating sub-arrays.

C. Contribution

Specifically, the main contributions of this paper are summarized as follows:

- Firstly, we propose a fresh RIS architecture built on sub-arrays. This new design partitions the active reflecting elements into multiple sub-arrays. Each sub-array can be independently switched on and off. This novel design entitles the RIS configuration with higher flexibility and can effectively reduce the non-transmit power due to the active components (e.g. amplifiers and phase-shifters). Although the *sub-array* structure has ever appeared in several latest works [18], [20], [33], their considerations are fundamentally different with ours. Specifically, [20] studies associating sub-arrays of passive RIS to different users. The sub-arrays considered in [18] and [33] are not switchable and hence does not involve activation control. To our best knowledge, activation control of sub-arrays of active-RIS has never been investigated in the existing literature.
- Based on our newly proposed sub-array construction, we further propose a novel power minimization scheme by jointly optimizing the sub-array activation control and the beamforming design. This scheme can effectively shut down the sub-arrays having poor channel conditions and retrench their power expenditure. Compared to the conventional RIS-aided power minimization considered in the existing literature, e.g., [5], [7], [33], our task becomes much more challenging due to the combinatorial

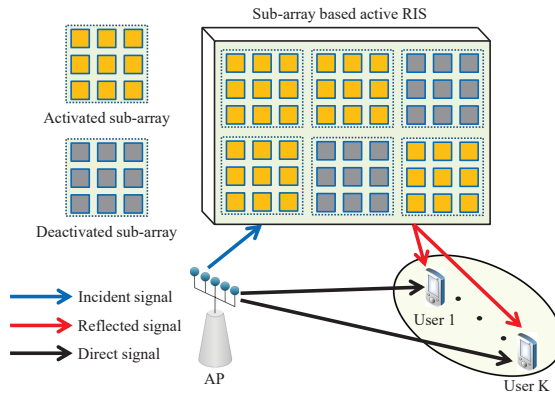


Fig. 2. An active RIS aided MU-MISO system based on sub-array.

nature of the sub-array activation control. Inspired by group sparsity inducing and majorization-minimization (MM) methodology, we develop a convergence guaranteed iterative solution that can achieve nearly optimal activation control with a very low complexity in activation pattern searching.

- Moreover, we investigate the EE maximization problem via jointly activating and controlling the sub-arrays of RIS, which has never been studied in relevant research on RIS. Specifically, the works [6], [18], [21] consider RIS-aided EE maximization without involving activation control and therefore their problems are much simpler than ours. Note that RIS activation control has been considered in optimizing EE in a multi-RIS context in the recent work [22]. Compared to [22], our proposed algorithm has much lower complexity in activation pattern searching and can achieve nearly optimal activation control.
- Furthermore, we also investigate the feasibility characterization of the power/EE optimization problem. Note that feasibility characterization of quality of service (QoS) requirements is highly meaningful in itself but generally overlooked in the existing literature, e.g., [20], [22], [31], [33]. This problem becomes more challenging under the sub-array activation consideration. This paper carefully studies this problem and proposes a converged algorithm to solve it.
- Last but not least, extensive numerical results are presented to verify the effectiveness of our sub-array activation control solutions and demonstrate the great benefit of the proposed sub-array architecture. Especially, our proposed low-complexity activation schemes perform nearly identical with exhaustive search methods, which are seldom compared in the existing relevant literature, e.g., [25]-[27], [29] and [31].

II. SYSTEM MODEL AND PROBLEM FORMULATION

A. System Model

As illustrated in Fig. 2, we consider a downlink system where an AP equipped with M_{AP} antennas serves K single-antenna users with the assistance of an active RIS containing

N_{RIS} reflecting elements. We denote $\mathcal{K} \triangleq \{1, \dots, K\}$ and $\mathcal{N} \triangleq \{1, \dots, N_{\text{RIS}}\}$ as the sets of users and reflecting elements, respectively.

Suppose that the active reflecting elements are grouped into M_{RIS} sub-arrays. Each sub-array consists of L_{RIS} reflecting elements. Thus, the total number of reflecting elements N_{RIS} is given by $N_{\text{RIS}} = M_{\text{RIS}}L_{\text{RIS}}$. Define $\mathcal{M} \triangleq \{1, \dots, M_{\text{RIS}}\}$ as the set of sub-arrays. The reflecting coefficient of the m th sub-array can be expressed as $\theta_m \triangleq [\beta_{(m-1)L_{\text{RIS}}+1}e^{j\theta_{(m-1)L_{\text{RIS}}+1}}, \dots, \beta_{mL_{\text{RIS}}}e^{j\theta_{mL_{\text{RIS}}}}]^T$, $m \in \mathcal{M}$, where β_n , $n \in \mathcal{N}$, indicates the amplifier coefficient and $\theta_n \in [0, 2\pi)$, $n \in \mathcal{N}$, denotes the phase shift of the n th reflecting element. Taking the limited magnifying capability of amplifiers into account, we have $\beta_n \in (0, \beta_{n,\max}]$, $n \in \mathcal{N}$, with $\beta_{n,\max}$, $n \in \mathcal{N}$, denoting the maximal magnifying factor of the n th amplifier. Furthermore, define $\Theta \triangleq \text{blkdiag}\{\Theta_1, \dots, \Theta_{M_{\text{RIS}}}\}$ as the reflecting coefficient matrix of the RIS, where $\Theta_m \triangleq \text{Diag}(\theta_m)$, $m \in \mathcal{M}$. Besides, we define $\mathcal{A} \subseteq \mathcal{M}$ as the set of activated sub-arrays. If $i \in \mathcal{A}$, then the i th sub-array is switched on, i.e., $\Theta_i \neq \mathbf{O}_{L_{\text{RIS}}}$. Otherwise, $\Theta_i = \mathbf{O}_{L_{\text{RIS}}}$ with $\mathbf{O}_{L_{\text{RIS}}}$ indicating an all-zero $L_{\text{RIS}} \times L_{\text{RIS}}$ matrix. Note that when setting each sub-array containing only one element, i.e., $L_{\text{RIS}} = 1$, our aforementioned model reduces to an element-wise activation scheme.

Denote $\mathbf{G} \in \mathbb{C}^{N_{\text{RIS}} \times M_{\text{AP}}}$, $\mathbf{h}_{d,k}^H \in \mathbb{C}^{1 \times M_{\text{AP}}}$, $k \in \mathcal{K}$, and $\mathbf{h}_{r,k}^H \in \mathbb{C}^{1 \times N_{\text{RIS}}}$, $k \in \mathcal{K}$, as the channels from the AP to the RIS, from the AP to the k th user and from the RIS to the k th user, respectively. Here we assume that the channel state information (CSI) is available, which can be obtained via cutting-the-edge channel estimation techniques [34]-[37].

The transmitted signal from the AP is given by

$$\mathbf{x}_{\text{AP}} = \sum_{k=1}^K \mathbf{f}_k x_k, \quad (1)$$

where $x_k \in \mathbb{C}$, $k \in \mathcal{K}$, stands for the signal transmitted to the k th user and $\mathbf{f}_k \in \mathbb{C}^{M_{\text{AP}}}$, $k \in \mathcal{K}$, represents the associated beamformer. Without loss of generality, assume $\mathbb{E}\{x_k\} = 0$, $\mathbb{E}\{|x_k|^2\} = 1$. Besides, it is reasonable to assume that different x_k 's are mutually uncorrelated.

According to the channels defined above, the received signal of the RIS can be expressed as

$$\mathbf{y}_{\text{RIS}} = \mathbf{G}\mathbf{x}_{\text{AP}} + \mathbf{n}_{\text{RIS}}, \quad (2)$$

where $\mathbf{n}_{\text{RIS}} \in \mathbb{C}^{N_{\text{RIS}}}$ is the thermal noise at the RIS with $\mathbf{n}_{\text{RIS}} \sim \mathcal{CN}(\mathbf{0}, \sigma_{\text{RIS}}^2 \mathbf{I}_{N_{\text{RIS}}})$ and $\mathbf{I}_{N_{\text{RIS}}}$ indicates an $N_{\text{RIS}} \times N_{\text{RIS}}$ identity matrix.

The incoming signal at the RIS will be reflected and amplified via the RIS. We can obtain the reflected signal from the RIS as follows

$$\mathbf{y}_k = \mathbf{h}_{r,k}^H \mathbf{y}_{\text{RIS}} + \mathbf{h}_{d,k}^H \mathbf{x}_{\text{AP}} + n_k, \quad k \in \mathcal{K}, \quad (3)$$

The k th user simultaneously receives the signals from the AP and the RIS, which reads as

$$y_k = \mathbf{h}_{r,k}^H \mathbf{y}_{\text{RIS}} + \mathbf{h}_{d,k}^H \mathbf{x}_{\text{AP}} + n_k, \quad k \in \mathcal{K}, \quad (4)$$

where $n_k \in \mathbb{C}$, $k \in \mathcal{K}$, denotes the thermal noise at the k th user. For simplicity, we suppose that $n_k \sim \mathcal{CN}(0, \sigma_k^2)$, $k \in \mathcal{K}$, and each n_k is uncorrelated with other n_j , $j \in \mathcal{K}$, $j \neq k$.

From (4), the signal-to-interference-plus-noise ratio (SINR) of the k th user can be given as

$$\text{SINR}_k(\mathbf{F}, \Theta) = \frac{|\mathbf{h}_k^H \mathbf{f}_k|^2}{\sum_{j=1, j \neq k}^K |\mathbf{h}_k^H \mathbf{f}_j|^2 + \sigma_{\text{RIS}}^2 \|\Theta^H \mathbf{h}_{r,k}\|_2^2 + \sigma_k^2}, \quad k \in \mathcal{K}, \quad (5)$$

where $\mathbf{F} \triangleq \{\mathbf{f}_k\}_{k=1}^K$ and $\mathbf{h}_k^H \triangleq \mathbf{h}_{r,k}^H \Theta \mathbf{G} + \mathbf{h}_{d,k}^H$, $k \in \mathcal{K}$, is the equivalent channel between the AP and the k th user.

Based on the above exposition, the achievable rate of the network is

$$R_{\text{total}}(\mathbf{F}, \Theta) = \sum_{k=1}^K \log(1 + \text{SINR}_k(\mathbf{F}, \Theta)). \quad (6)$$

Besides, as previously discussed, $\boldsymbol{\theta}_i$ will be a zero vector if the i th sub-array is turned off. Therefore, by denoting $\tilde{\boldsymbol{\theta}} \triangleq [\|\boldsymbol{\theta}_1\|_2, \dots, \|\boldsymbol{\theta}_{M_{\text{RIS}}}\|_2]^T$, the number of activated sub-arrays $|\mathcal{A}|$ can be equivalently written as

$$|\mathcal{A}| = \|\tilde{\boldsymbol{\theta}}\|_0, \quad (7)$$

where the ℓ_0 -norm counts the number of the non-zero elements of the input vector.

B. Power Consumption Model

In this subsection, we will discuss the power consumption model involving sub-array activation.

Firstly, the power consumption at the AP is given by

$$P_{\text{AP}}(\mathbf{F}) = \xi_{\text{AP}} \sum_{k=1}^K \|\mathbf{f}_k\|_2^2 + P_{c,\text{AP}}, \quad (8)$$

where ξ_{AP} stands for the inverse of the emission efficiency of the AP, $P_{c,\text{AP}}$ represents the energy consumed by signal processing (e.g. by CPU and SRAM), RF chain components (e.g. ADCs/DACs, mixers, phase shifters, oscillators), hardware peripherals and so on [38].

Secondly, the power consumption at the RIS reads as

$$P_{\text{RIS}}(\mathbf{F}, \Theta) = \xi_{\text{RIS}} \left(\sum_{k=1}^K \|\Theta \mathbf{G} \mathbf{f}_k\|_2^2 + \sigma_{\text{RIS}}^2 \|\Theta\|_F^2 \right) + \|\tilde{\boldsymbol{\theta}}\|_0 L_{\text{RIS}} P_{c,\text{RIS}}, \quad (9)$$

where ξ_{RIS} stands for the inverse of the emission efficiency of the RIS amplifiers. Generally, $P_{c,\text{RIS}}$ is viewed as a constant [16].

Lastly, the total power consumption of users can be calculated as follows

$$P_{\text{user}} = \sum_{k=1}^K P_{c,k}, \quad (10)$$

where $P_{c,k}$, $k \in \mathcal{K}$, indicates the dissipated power at the k th user, which are generally regarded as constants for downlink scenarios [6], [18], [20].

To sum up, the total power consumption of the considered system is given by

$$P_{\text{total}}(\mathbf{F}, \Theta) = P_{\text{AP}}(\mathbf{F}) + P_{\text{RIS}}(\mathbf{F}, \Theta) + P_{\text{user}}. \quad (11)$$

C. Problem Formulation

1) Power minimization

To reduce power consumption, we propose to jointly design sub-array activation and beamforming of the AP and the RIS while guaranteeing the QoS requirement for each user, which can be formulated as

$$(\mathcal{P}1) : \min_{\mathbf{F}, \Theta} P_{\text{total}}(\mathbf{F}, \Theta) \quad (12)$$

$$\text{s.t. } \sum_{k=1}^K \|\mathbf{f}_k\|_2^2 \leq P_{\text{AP,max}}, \quad (12a)$$

$$P_{\text{RIS}}(\mathbf{F}, \Theta) \leq P_{\text{RIS,max}}, \quad (12b)$$

$$\log(1 + \text{SINR}_k(\mathbf{F}, \Theta)) \geq R_k, \quad k \in \mathcal{K}, \quad (12c)$$

$$\beta_n \leq \beta_{n,\text{max}}, \quad \theta_n \in [0, 2\pi], \quad n \in \mathcal{N}, \quad (12d)$$

where $P_{\text{AP,max}}$ in (12a) and $P_{\text{RIS,max}}$ in (12b) represent the power supply at the AP and the RIS, respectively, and (12c) states the QoS constraints for all users.

2) Energy efficiency maximization

Another highly concerned performance metric is EE, whose optimization can be formulated as the following problem [6]

$$(\mathcal{P}2) : \max_{\mathbf{F}, \Theta} \frac{R_{\text{total}}(\mathbf{F}, \Theta)}{P_{\text{total}}(\mathbf{F}, \Theta)} \quad (13)$$

$$\text{s.t. } \sum_{k=1}^K \|\mathbf{f}_k\|_2^2 \leq P_{\text{AP,max}}, \quad (13a)$$

$$P_{\text{RIS}}(\mathbf{F}, \Theta) \leq P_{\text{RIS,max}}, \quad (13b)$$

$$\log(1 + \text{SINR}_k(\mathbf{F}, \Theta)) \geq R_k, \quad k \in \mathcal{K}, \quad (13c)$$

$$\beta_n \leq \beta_{n,\text{max}}, \quad \theta_n \in [0, 2\pi], \quad n \in \mathcal{N}. \quad (13d)$$

The problems $(\mathcal{P}1)$ and $(\mathcal{P}2)$ are both challenging due to their highly non-convex objectives/constraints and the combinatorial nature caused by the sub-array activation.

III. SOLUTION TO POWER MINIMIZATION PROBLEM

In this section, we develop a solution to solve $(\mathcal{P}1)$.

A. Approximation and Group Sparsity Inducing

Firstly, it can be observed that the main difficulty to solve $(\mathcal{P}1)$ comes from the term $\|\tilde{\boldsymbol{\theta}}\|_0$, which is non-convex and non-smooth. Note that once the activation set \mathcal{A} is given, the ℓ_0 -norm term becomes constant and hence the problem $(\mathcal{P}1)$ boils down to a conventional power minimization problem. However, exhaustively searching all $(2^{M_{\text{RIS}}} - 1)$ possible sub-array activation patterns will yield unrealistically high complexity.

To deal with the non-smoothness of $\|\tilde{\boldsymbol{\theta}}\|_0$, we adopt smooth approximations to surrogate the ℓ_0 -norm. In fact, a bunch of well-behaved smooth functions have been found to accomplish this goal [39], including parameterized logarithm/exponential/arctangent functions, which can all be further tackled by the majorization-minimization (MM) method [40] and exhibit similar performance [39]. In the following, logarithm function will be selected to approximate ℓ_0 -norm. In particular, the ℓ_0 -norm can be smoothed by

$$\|\tilde{\boldsymbol{\theta}}\|_0 \approx \sum_{m=1}^{M_{\text{RIS}}} \frac{\log \left(\frac{\|\boldsymbol{\theta}_m\|_2}{\delta} + 1 \right)}{\log \left(\frac{1}{\delta} + 1 \right)}, \quad (14)$$

where the parameter δ is a predefined positive constant and controls the approximation precision, whose value is typically

set within the range $[10^{-6}, 10^{-5}]$ to yield a satisfying approximation.

Define $\tilde{P}_{\text{RIS}}(\mathbf{F}, \Theta)$ and $\tilde{P}_{\text{total}}(\mathbf{F}, \Theta)$ as the functions after substituting (14) into (9) and (11), respectively. In the following, we focus on solving the approximated problem as follows

$$(\mathcal{P}3) : \min_{\mathbf{F}, \Theta} \tilde{P}_{\text{total}}(\mathbf{F}, \Theta) \quad (15)$$

$$\text{s.t. } \sum_{k=1}^K \|\mathbf{f}_k\|_2^2 \leq P_{\text{AP,max}}, \quad (15a)$$

$$\tilde{P}_{\text{RIS}}(\mathbf{F}, \Theta) \leq P_{\text{RIS,max}}, \quad (15b)$$

$$\log(1 + \text{SINR}_k(\mathbf{F}, \Theta)) \geq R_k, \quad k \in \mathcal{K}, \quad (15c)$$

$$\beta_n \leq \beta_{n,\max}, \quad \theta_n \in [0, 2\pi], \quad n \in \mathcal{N}. \quad (15d)$$

This problem is still difficult to tackle due to the intractable rate function in (15c). We adopt the weighted minimal mean square error (WMMSE) method [41] to transform it into a more tractable form as follows. According to [41], for $k \in \mathcal{K}$, we have

$$\begin{aligned} \log(1 + \text{SINR}_k(\mathbf{F}, \Theta)) &= \max_{w_k} \{ \log(w_k) - w_k \tilde{\mathbf{e}}_k(\mathbf{F}, \Theta) + 1 \} \\ &= \max_{w_k, v_k} \{ \log(w_k) - w_k \mathbf{e}_k(\mathbf{v}, \mathbf{F}, \Theta) + 1 \} \triangleq \max_{w_k, v_k} \tilde{R}_k(\mathbf{v}, \mathbf{w}, \mathbf{F}, \Theta), \end{aligned} \quad (16)$$

where functions $\tilde{\mathbf{e}}_k(\mathbf{F}, \Theta)$ and $\mathbf{e}_k(\mathbf{v}, \mathbf{F}, \Theta)$ are given by

$$\tilde{\mathbf{e}}_k(\mathbf{F}, \Theta) = \Upsilon_k^{-1}(\mathbf{F}, \Theta) \mathbf{h}_k^H \mathbf{f}_k, \quad (17)$$

$$\mathbf{e}_k(\mathbf{v}, \mathbf{F}, \Theta) = v_k^* \Upsilon_k(\mathbf{F}, \Theta) v_k - 2\text{Re}\{v_k^* \mathbf{h}_k^H \mathbf{f}_k\} + 1, \quad (18)$$

$$\Upsilon_k(\mathbf{F}, \Theta) \triangleq \sum_{j=1}^K |\mathbf{h}_k^H \mathbf{f}_j|^2 + \sigma_{\text{RIS}}^2 \|\Theta^H \mathbf{h}_{r,k}\|_2^2 + \sigma_k^2, \quad (19)$$

$\mathbf{w} = [w_1, \dots, w_K]^T$ and $\mathbf{v} = [v_1, \dots, v_K]^T$ are auxiliary variables introduced by WMMSE. The maximization in (16) can be achieved when \mathbf{v} and \mathbf{w} satisfy the equalities (21) and (22), respectively. Detailed reasoning of (16) can be found in [41].

Based on the above transformation, $(\mathcal{P}3)$ can be equivalently written as

$$(\mathcal{P}4) : \min_{\mathbf{F}, \Theta, \mathbf{w}, \mathbf{v}} \tilde{P}_{\text{total}}(\mathbf{F}, \Theta) \quad (20)$$

$$\text{s.t. } \sum_{k=1}^K \|\mathbf{f}_k\|_2^2 \leq P_{\text{AP,max}}, \quad (20a)$$

$$\tilde{P}_{\text{RIS}}(\mathbf{F}, \Theta) \leq P_{\text{RIS,max}}, \quad (20b)$$

$$\tilde{R}_k(\mathbf{v}, \mathbf{w}, \mathbf{F}, \Theta) \geq R_k, \quad k \in \mathcal{K}, \quad (20c)$$

$$\beta_n \leq \beta_{n,\max}, \quad \theta_n \in [0, 2\pi], \quad n \in \mathcal{N}. \quad (20d)$$

Here, we briefly clarify the equivalence between $(\mathcal{P}3)$ and $(\mathcal{P}4)$. Suppose $\tilde{\mathbf{F}}$ and $\tilde{\Theta}$ are feasible to $(\mathcal{P}4)$, then there exist $\tilde{\mathbf{v}}$ and $\tilde{\mathbf{w}}$ such that $\tilde{R}_k(\tilde{\mathbf{v}}, \tilde{\mathbf{w}}, \tilde{\mathbf{F}}, \tilde{\Theta}) \geq R_k$, $k \in \mathcal{K}$. According to (16), $\log(1 + \text{SINR}_k(\tilde{\mathbf{F}}, \tilde{\Theta})) \geq \tilde{R}_k(\tilde{\mathbf{v}}, \tilde{\mathbf{w}}, \tilde{\mathbf{F}}, \tilde{\Theta}) \geq R_k$, $k \in \mathcal{K}$, which means that $\tilde{\mathbf{F}}$ and $\tilde{\Theta}$ are also feasible to $(\mathcal{P}3)$. Conversely, if $\tilde{\mathbf{F}}$ and $\tilde{\Theta}$ are feasible to $(\mathcal{P}3)$, then by (16), $\tilde{R}_k(\hat{\mathbf{v}}, \hat{\mathbf{w}}, \hat{\mathbf{F}}, \hat{\Theta}) = \log(1 + \text{SINR}_k(\hat{\mathbf{F}}, \hat{\Theta})) \geq R_k$ with $\hat{\mathbf{v}}$ and $\hat{\mathbf{w}}$ satisfying (21) and (22), respectively. Therefore, the feasible domains of \mathbf{F} and Θ associated with $(\mathcal{P}3)$ and $(\mathcal{P}4)$ coincide, which proves the equivalence.

In the following, we adopt the block coordinate descent (BCD) method to resolve the above problem $(\mathcal{P}4)$.

1) Optimize auxiliary variable \mathbf{v}

With other variables being fixed, this subproblem is actually a feasibility check problem due to the absence of the objective function, which can be equivalently transformed into

$\max_{\mathbf{v}} (\log(w_k) - w_k \mathbf{e}_k(\mathbf{v}, \mathbf{F}, \Theta))$, $k \in \mathcal{K}$. This is an unconstrained convex quadratic problem and by setting the first-order derivative equal to zero, its optimal solution can be expressed as

$$v_k = \frac{\mathbf{h}_k^H \mathbf{f}_k}{\sum_{j=1}^K |\mathbf{h}_k^H \mathbf{f}_j|^2 + \sigma_{\text{RIS}}^2 \|\Theta^H \mathbf{h}_{r,k}\|_2^2 + \sigma_k^2}, \quad k \in \mathcal{K}. \quad (21)$$

2) Optimize auxiliary variable \mathbf{w}

Following the similar argument as that for updating \mathbf{v} , the optimization of \mathbf{w} can also be converted into a non-constrained convex problem, whose optimal solution can be readily obtained as

$$w_k = \mathbf{e}_k^{-1}(\mathbf{v}, \mathbf{F}, \Theta), \quad k \in \mathcal{K}. \quad (22)$$

3) Optimize beamforming at the AP \mathbf{F}

With other variables given, the update of \mathbf{F} reduces to solving the following problem

$$(\mathcal{P}5) : \min_{\mathbf{F}} \xi_{\text{AP}} \sum_{k=1}^K \|\mathbf{f}_k\|_2^2 + \xi_{\text{RIS}} \sum_{k=1}^K \|\Theta \mathbf{G} \mathbf{f}_k\|_2^2 \quad (23)$$

$$\text{s.t. } \sum_{k=1}^K \|\mathbf{f}_k\|_2^2 \leq P_{\text{AP,max}}, \quad (23a)$$

$$\begin{aligned} &\xi_{\text{RIS}} \left(\sum_{k=1}^K \|\Theta \mathbf{G} \mathbf{f}_k\|_2^2 + \sigma_{\text{RIS}}^2 \|\Theta\|_F^2 \right) \\ &+ \sum_{m=1}^{M_{\text{RIS}}} \frac{\log \left(\frac{\|\boldsymbol{\theta}_m\|_2}{\delta} + 1 \right)}{\log \left(\frac{1}{\delta} + 1 \right)} L_{\text{RIS}} P_{c,\text{RIS}} \leq P_{\text{RIS,max}}, \end{aligned} \quad (23b)$$

$$\begin{aligned} &\log(w_k) - w_k \left(v_k^* \left(\sum_{j=1}^K |\mathbf{h}_k^H \mathbf{f}_j|^2 + \sigma_{\text{RIS}}^2 \|\Theta^H \mathbf{h}_{r,k}\|_2^2 \right. \right. \\ &\left. \left. + \sigma_k^2 \right) v_k - 2\text{Re}\{v_k^* \mathbf{h}_k^H \mathbf{f}_k\} + 1 \right) + 1 \geq R_k, \quad k \in \mathcal{K}, \end{aligned} \quad (23c)$$

which is a second order cone programming (SOCP) [42] and can be solved by numerical solvers, such as CVX [43].

4) Optimize the RIS configuration Θ

Finally, we proceed to optimize Θ . The difficulty lies in the non-convexity of the right hand side of (14). To cope with this issue, we invoke MM method to convexify it [40]. Specifically, noticing the concavity of logarithm function, we perform its linearization at the point of $\boldsymbol{\theta}^{(t)}$ to obtain a convex tight upper-bound, shown as follows

$$\begin{aligned} \log \left(\frac{\|\boldsymbol{\theta}_m\|_2}{\delta} + 1 \right) &\leq \log \left(\frac{\|\boldsymbol{\theta}_m^{(t)}\|_2}{\delta} + 1 \right) + \frac{\|\boldsymbol{\theta}_m\|_2 - \|\boldsymbol{\theta}_m^{(t)}\|_2}{\|\boldsymbol{\theta}_m^{(t)}\|_2 + \delta} \\ &\triangleq g_m(\boldsymbol{\theta}|\boldsymbol{\theta}^{(t)}), \quad m \in \mathcal{M}. \end{aligned} \quad (24)$$

Substituting (14) by (24) and utilizing the facts that $\|\Theta \mathbf{G} \mathbf{f}_k\|_2^2 = \boldsymbol{\theta}^T \text{Diag}(\mathbf{G} \mathbf{f}_k)(\text{Diag}(\mathbf{G} \mathbf{f}_k))^H \boldsymbol{\theta}^*$, $\|\Theta\|_F^2 = \boldsymbol{\theta}^T \boldsymbol{\theta}^*$, $\|\Theta^H \mathbf{h}_{r,k}\|_2^2 = \boldsymbol{\theta}^T \text{Diag}(\mathbf{h}_{r,k}^H) \text{Diag}(\mathbf{h}_{r,k}) \boldsymbol{\theta}^*$ and $\mathbf{h}_{r,k}^H \Theta \mathbf{G} \mathbf{f}_k = \boldsymbol{\theta}^T \text{Diag}(\mathbf{h}_{r,k}^H) \mathbf{G} \mathbf{f}_k$, after some manipulations, the compact form of the subproblem w.r.t. $\boldsymbol{\theta}$ is given as follows

$$(\mathcal{P}6) : \min_{\boldsymbol{\theta}} \boldsymbol{\theta}^T \mathbf{P} \boldsymbol{\theta}^* + g(\boldsymbol{\theta}|\boldsymbol{\theta}^{(t)}) L_{\text{RIS}} P_{c,\text{RIS}} \quad (25)$$

$$\text{s.t. } \boldsymbol{\theta}^T \mathbf{P} \boldsymbol{\theta}^* + g(\boldsymbol{\theta}|\boldsymbol{\theta}^{(t)}) L_{\text{RIS}} P_{c,\text{RIS}} \leq P_{\text{RIS,max}}, \quad (25a)$$

$$\boldsymbol{\theta}^T \mathbf{Q}_k \boldsymbol{\theta}^* + 2\text{Re}\{\mathbf{q}_k^H \boldsymbol{\theta}^*\} + q_k \leq r_k, \quad k \in \mathcal{K}, \quad (25b)$$

$$|\theta_n| \leq \beta_{n,\max}, \quad n \in \mathcal{N}, \quad (25c)$$

Algorithm 1: Solving the problem $(\mathcal{P}4)$

- 1: Initialize $\mathbf{F}^{(0)}$, $\Theta^{(0)}$ (via Alg. 5) and $t = 0$;
- 2: **repeat**
- 3: update $\mathbf{v}^{(t+1)}$ by function (21);
- 4: update $\mathbf{w}^{(t+1)}$ by function (22);
- 5: update $\mathbf{F}^{(t+1)}$ by solving $(\mathcal{P}5)$;
- 6: update $\Theta^{(t+1)}$ by solving $(\mathcal{P}6)$;
- 7: $t := t + 1$;
- 8: **until** convergence

where the parameters are given as

$$\begin{aligned} \mathbf{H}_{r,k} &\triangleq \text{Diag}(\mathbf{h}_{r,k}^H), \bar{\mathbf{q}}_{k,j} \triangleq \mathbf{H}_{r,k} \mathbf{G} \mathbf{f}_j, \bar{q}_{k,j} \triangleq v_k^* \mathbf{h}_{d,k}^H \mathbf{f}_j, \\ \bar{\mathbf{Q}}_{k,j} &\triangleq \mathbf{H}_{r,k} \mathbf{G} \mathbf{f}_j \mathbf{f}_j^H \mathbf{G}^H \mathbf{H}_{r,k}^H, r_k \triangleq \log(w_k) - R_k + 1, \\ \mathbf{P} &= \xi_{\text{RIS}} \left(\sum_{k=1}^K \text{Diag}(\mathbf{G} \mathbf{f}_k) (\text{Diag}(\mathbf{G} \mathbf{f}_k))^H + \sigma_{\text{RIS}}^2 \mathbf{I}_{N_{\text{RIS}}} \right), \\ \mathbf{Q}_k &= w_k \left(\sum_{j=1}^K v_k^* \bar{\mathbf{Q}}_{k,j} v_k + \sigma_{\text{RIS}}^2 v_k^* \mathbf{H}_{r,k} \mathbf{H}_{r,k}^H v_k \right), \\ \mathbf{q}_k^H &= w_k \left(\sum_{j=1}^K \bar{q}_{k,j} \bar{\mathbf{q}}_{k,j}^H v_k - \bar{\mathbf{q}}_{k,k}^H v_k \right), \\ q_k &= w_k \left(1 - 2\text{Re}\{\bar{q}_{k,k}\} + \sum_{j=1}^K |\bar{q}_{k,j}|^2 + \sigma_k^2 |v_k|^2 \right), \\ g(\boldsymbol{\theta}|\boldsymbol{\theta}^{(t)}) &= \frac{\sum_{m=1}^{M_{\text{RIS}}} g_m(\boldsymbol{\theta}|\boldsymbol{\theta}^{(t)})}{\log\left(\frac{1}{\delta} + 1\right)}. \end{aligned} \quad (26)$$

The problem $(\mathcal{P}6)$ is convex and can be numerically solved.

The overall algorithm for $(\mathcal{P}4)$ is given in Algorithm 1. The following theorem characterizes the convergence of Alg. 1, which is proved in Appendix A.

Theorem 1. Assume that Alg. 1 starts from a feasible point, then the solution iterates generated by Alg. 1 maintain feasible to $(\mathcal{P}4)$ and yields monotonically decreasing objective values of $(\mathcal{P}4)$.

B. Determine Activation Pattern

Based on the obtained solution $\boldsymbol{\theta}^*$, we proceed to determine the activation pattern of the sub-arrays.

It is worth noting that the solution $\boldsymbol{\theta}^*$ has a group sparsity structure, i.e., some sub-arrays have values several orders of multitudes smaller than others. The reason lies in that, if $\|\boldsymbol{\theta}_m^{(t)}\|_2$, $m \in \mathcal{M}$, is small, then, in the $(t+1)$ th iteration, the weighting factor $1/(\|\boldsymbol{\theta}_m^{(t)}\|_2 + \delta)$ will be large, which will further push $\|\boldsymbol{\theta}_m\|_2$ towards zero [44]. Intuitively, the smaller magnitude $\|\boldsymbol{\theta}_m^*\|_2$ a sub-array has, the less it contributes to the QoS requirements, which implies that it should be switched off with a higher priority. Inspired by this fact and sorting $\|\boldsymbol{\theta}_m\|_2$, $m \in \mathcal{M}$, in an ascending order, we obtain a “switch-off” ranking $\{\pi_1, \dots, \pi_{M_{\text{RIS}}}\}$ such that $\|\boldsymbol{\theta}_{\pi_1}^*\|_2 \leq \dots \leq \|\boldsymbol{\theta}_{\pi_{M_{\text{RIS}}}}^*\|_2$. The π_i with a smaller i has a higher priority to be deactivated. Here we propose to always turn off the sub-arrays with highest switch-off priorities. That is, the active set should be $\mathcal{A}(J) = \{\pi_{J+1}, \pi_{J+2}, \dots, \pi_{M_{\text{RIS}}}\}$ and we wish to determine the maximal J . Specifically, we adopt bi-section search to iteratively locate the maximal splitting point J , which partitions \mathcal{M} into activated and deactivated sets. For the active

Algorithm 2: Solution to $(\mathcal{P}1)$

- 1: Invoke Alg. 1 to obtain $\boldsymbol{\theta}^*$ and ranking $\{\pi_i\}_{i=1}^{M_{\text{RIS}}}$;
- 2: Set $J_{\min} = 0$ and $J_{\max} = M_{\text{RIS}}$;
- 3: **repeat**
- 4: set $J = \lfloor \frac{J_{\min}+J_{\max}}{2} \rfloor$, $\mathcal{A}(J) = \{\pi_{J+1}, \dots, \pi_{M_{\text{RIS}}}\}$;
- 5: **if** $(\mathcal{P}_{\mathcal{A}(J)})$ is feasible **then**
- 6: $J_{\min} = J$;
- 7: **else**
- 8: $J_{\max} = J$;
- 9: **end if**
- 10: **until** $J_{\max} - J_{\min} = 1$
- 11: Obtain $\mathcal{A}(J_{\min}) = \{\pi_{J_{\min}+1}, \dots, \pi_{M_{\text{RIS}}}\}$ and perform power minimization via calling Alg. 1.

set $\mathcal{A}(J)$ associated with given J , we attempt to solve the following feasibility characterization problem:

$$(\mathcal{P}_{\mathcal{A}(J)}): \text{Find } (\mathbf{F}, \Theta_{m \in \mathcal{A}(J)}) \quad (27)$$

$$\text{s.t. } \sum_{k=1}^K \|\mathbf{f}_k\|_2^2 \leq P_{\text{AP,max}}, \quad (27a)$$

$$\mathbf{P}_{\text{RIS}}(\mathbf{F}, \Theta_{m \in \mathcal{A}(J)}) \leq P_{\text{RIS,max}}, \quad (27b)$$

$$\log(1 + \text{SINR}_k(\mathbf{F}, \Theta_{m \in \mathcal{A}(J)})) \geq R_k, k \in \mathcal{K}, \quad (27c)$$

$$\beta_n \leq \beta_{n,\max}, \theta_n \in [0, 2\pi], n \in \mathcal{N}, \quad (27d)$$

whose solution will be discussed in Sec. V. If $(\mathcal{P}_{\mathcal{A}(J)})$ is feasible, then more sub-arrays can be deactivated in the next iteration. Otherwise, we have to turn on more sub-arrays to achieve QoS constraints. Once the activated pattern is determined, the ℓ_0 -norm in $(\mathcal{P}1)$ becomes a constant and hence we need only consider the configurations of the activated sub-arrays and the AP's beamforming, which can be optimized via invoking Alg. 1 again.

The overall procedure to solve $(\mathcal{P}1)$ is summarized in Algorithm 2.

C. Computational Complexity Analysis

Majority of the complexity of solving $(\mathcal{P}4)$ lies in solving the problems $(\mathcal{P}5)$ and $(\mathcal{P}6)$, which result in $\mathcal{O}(K^{4.5} M_{\text{AP}}^3)$ and $\mathcal{O}((K + N_{\text{RIS}})^{1.5} N_{\text{RIS}}^3)$, respectively. Hence, the total complexity of Alg. 1 approximately has an order of $\mathcal{O}_1 = \mathcal{O}(T_1(K^{4.5} M_{\text{AP}}^3 + (K + N_{\text{RIS}})^{1.5} N_{\text{RIS}}^3))$, where T_1 represents the number of iterations to tackle $(\mathcal{P}4)$. Besides, Alg. 2 invokes at most $\log_2(M_{\text{RIS}})$ times of Alg. 5, which leads to the complexity of $\mathcal{O}_2 = 2\mathcal{O}_1 + \log_2(M_{\text{RIS}})\mathcal{O}_5$, where \mathcal{O}_5 stands for the complexity of Alg. 5 given in Sec. V.

IV. SOLUTION TO EE MAXIMIZATION PROBLEM

In this section, we present the maximization of EE. Particularly, the troublesome activation pattern and the fractional form of (13) makes the problem more challenging.

A. Approximation and Transformation

To tackle $(\mathcal{P}2)$, following the similar arguments used in power minimization, we adopt the approximation of ℓ_0 -norm in (14) and leverage the WMMSE method to transform it into the following problem

$$(\mathcal{P}7): \max_{\mathbf{F}, \Theta, \mathbf{w}, \mathbf{v}} \frac{\sum_{k=1}^K \tilde{\mathbf{R}}_k(\mathbf{v}, \mathbf{w}, \mathbf{F}, \Theta)}{\tilde{\mathbf{P}}_{\text{total}}(\mathbf{F}, \Theta)} \quad (28)$$

$$\text{s.t. } \sum_{k=1}^K \|f_k\|_2^2 \leq P_{\text{AP,max}}, \quad (28a)$$

$$\tilde{P}_{\text{RIS}}(\mathbf{F}, \Theta) \leq P_{\text{RIS,max}}, \quad (28b)$$

$$\tilde{R}_k(\mathbf{v}, \mathbf{w}, \mathbf{F}, \Theta) \geq R_k, \quad k \in \mathcal{K}, \quad (28c)$$

$$\beta_n \leq \beta_{n,\text{max}}, \quad \theta_n \in [0, 2\pi), \quad n \in \mathcal{N}. \quad (28d)$$

(P7) is still difficult to tackle due to the fractional objective (28). One appealing approach is the Dinkelbach's method [6], [21], [22]. However, this classical method requires, in each of its iteration, to globally optimizes the residual of the numerator deducted by the weighted denominator [45], which is indeed intractable for (P7). To overcome this difficulty, we equivalently rewrite (P7) via introducing slack variables $\mathbf{x} = [x_1, \dots, x_K]^T$ and y as follows

$$(\mathcal{P}8) : \max_{\mathbf{F}, \Theta, \mathbf{w}, \mathbf{v}, \mathbf{x} \geq 0, y} \frac{\sum_{k=1}^K x_k^2}{y} \quad (29)$$

$$\text{s.t. } \tilde{R}_k(\mathbf{v}, \mathbf{w}, \mathbf{F}, \Theta) \geq x_k^2, \quad k \in \mathcal{K}, \quad (29a)$$

$$\tilde{P}_{\text{total}}(\mathbf{F}, \Theta) \leq y, \quad (29b)$$

$$\sum_{k=1}^K \|f_k\|_2^2 \leq P_{\text{AP,max}}, \quad (29c)$$

$$\tilde{P}_{\text{RIS}}(\mathbf{F}, \Theta) \leq P_{\text{RIS,max}}, \quad (29d)$$

$$x_k^2 \geq R_k, \quad k \in \mathcal{K}, \quad (29e)$$

$$\beta_n \leq \beta_{n,\text{max}}, \quad \theta_n \in [0, 2\pi), \quad n \in \mathcal{N}. \quad (29f)$$

Notice that the function x^2/y is jointly convex in (x, y) and the constraint (29e) has the form of difference of convex functions (DCs). Therefore, motivated by successive convex approximation (SCA) [40], the following inequalities hold via the first-order Taylor expansion

$$\frac{x_k^2}{y} \geq \left(\frac{2x_k^{(t)}}{y^{(t)}} x_k - \frac{(x_k^{(t)})^2}{(y^{(t)})^2} y \right), \quad k \in \mathcal{K}, \quad (30)$$

$$x_k^2 \geq 2x_k^{(t)} x_k - (x_k^{(t)})^2, \quad k \in \mathcal{K}, \quad (31)$$

where $x_k^{(t)}$, $k \in \mathcal{K}$ and $y^{(t)}$ are the most up-to-date values of x_k , $k \in \mathcal{K}$ and y obtained in the t th iteration, respectively. Following the MM methodology, we convexify (P8) via replacing its objective (29) and constraint (29e) with the lower bounds developed in (30) and (31), respectively, which can be solved via the following BCD procedure.

1) Optimize auxiliary variable \mathbf{v}

It can be easily checked that the update of \mathbf{v} can still be obtained via (21).

2) Optimize auxiliary variable \mathbf{w}

Similarly, the closed-form solution (22) still apply for \mathbf{w} 's update.

3) Optimize beamforming at the AP \mathbf{F}

Next, we optimize AP's beamformer \mathbf{F} , which reduces to solve the following problem

$$(\mathcal{P}9) : \max_{\mathbf{F}, \mathbf{x} \geq 0, y} \sum_{k=1}^K \left(\frac{2x_k^{(t)}}{y^{(t)}} x_k - \frac{(x_k^{(t)})^2}{(y^{(t)})^2} y \right) \quad (32)$$

$$\text{s.t. } \tilde{R}_k(\mathbf{F}|\mathbf{v}, \mathbf{w}, \Theta) \geq x_k^2, \quad k \in \mathcal{K}, \quad (32a)$$

$$\tilde{P}_{\text{total}}(\mathbf{F}|\Theta) \leq y, \quad (32b)$$

$$\sum_{k=1}^K \|f_k\|_2^2 \leq P_{\text{AP,max}}, \quad (32c)$$

Algorithm 3: Solving the problem (P7)

- 1: Initialize $\mathbf{F}^{(0)}$, $\Theta^{(0)}$, $\mathbf{x}^{(0)}$, $y^{(0)}$ (via Alg. 5) and $t = 0$;
 - 2: **repeat**
 - 3: update $\mathbf{v}^{(t+1)}$ by function (21);
 - 4: update $\mathbf{w}^{(t+1)}$ by function (22);
 - 5: update $(\mathbf{F}^{(t+1)}, \mathbf{x}^{(t+\frac{1}{2})}, y^{(t+\frac{1}{2})})$ by solving (P9);
 - 6: update $(\Theta^{(t+1)}, \mathbf{x}^{(t+1)}, y^{(t+1)})$ by solving (P10);
 - 7: $t := t + 1$;
 - 8: **until** convergence
-

$$\tilde{P}_{\text{RIS}}(\mathbf{F}|\Theta) \leq P_{\text{RIS,max}}, \quad (32d)$$

$$2x_k^{(t)} x_k - (x_k^{(t)})^2 \geq R_k, \quad k \in \mathcal{K}, \quad (32e)$$

which is convex and can be solved by numerical solvers, e.g., CVX.

4) Optimize the RIS configuration Θ

To update Θ , we utilize the same tricks as used in solving (P6) to convexify the constraints (29b) and (29d) and mean to solve the following problem

$$(\mathcal{P}10) : \max_{\Theta, \mathbf{x} \geq 0, y} \sum_{k=1}^K \left(\frac{2x_k^{(t+\frac{1}{2})}}{y^{(t+\frac{1}{2})}} x_k - \frac{(x_k^{(t+\frac{1}{2})})^2}{(y^{(t+\frac{1}{2})})^2} y \right) \quad (33)$$

$$\text{s.t. } \boldsymbol{\theta}^T \mathbf{Q}_k \boldsymbol{\theta}^* + 2\text{Re}\{\mathbf{q}_k^H \boldsymbol{\theta}^*\} + q_k \leq \log(w_k) + 1 - x_k^2, \quad k \in \mathcal{K}, \quad (33a)$$

$$\boldsymbol{\theta}^T \mathbf{P} \boldsymbol{\theta}^* + g(\boldsymbol{\theta}|\boldsymbol{\theta}^{(t)}) L_{\text{RIS}} P_{\text{c,RIS}} + P_{\text{AP}} + P_{\text{user}} \leq y, \quad (33b)$$

$$\boldsymbol{\theta}^T \mathbf{P} \boldsymbol{\theta}^* + g(\boldsymbol{\theta}|\boldsymbol{\theta}^{(t)}) L_{\text{RIS}} P_{\text{c,RIS}} \leq P_{\text{RIS,max}}, \quad (33c)$$

$$2x_k^{(t+\frac{1}{2})} x_k - (x_k^{(t+\frac{1}{2})})^2 \geq R_k, \quad k \in \mathcal{K}, \quad (33d)$$

$$|\theta_n| \leq \beta_{n,\text{max}}, \quad n \in \mathcal{N}, \quad (33e)$$

where $(\mathbf{x}^{(t+\frac{1}{2})}, y^{(t+\frac{1}{2})})$ is obtained via solving (P9) and the notations above follow the definitions in (26). (P10) is a convex optimization problem and can be numerically solved.

The overall algorithm to tackle (P7) is summarized in Algorithm 3, which guarantees a feasible solution and monotonically converging objective, as pointed out by the theorem below proved in Appendix B:

Theorem 2. Assume that Alg. 3 starts from a feasible point, then the solution iterates generated by Alg. 3 maintain feasible to (P7) and yields monotonically increasing objective values of (P7).

B. Determine Activation Pattern

Similar to power minimization, we could obtain a ranking associated with $\tilde{\boldsymbol{\theta}}^*$ yielded by Alg. 3. Here we still activate the sub-arrays with the highest switch-off priorities as previously.

Unfortunately, the previous bi-section search to determine \mathcal{A} is not applicable anymore. The rationale is that, as opposed to the power control scenario, the number of activated sub-arrays does not affect the EE in a simple monotonic manner. Indeed, more turned-on sub-arrays will increase both the information rate (the numerator) and the power consumption (the denominator). Therefore, we search all the M_{RIS} possibilities, which yields a linear searching complexity.

Specifically, we start by $\mathcal{A} = \mathcal{M}$ and perform EE maximization. In each iteration, we deactivate the sub-array with highest switch-off priority in the current active set, check its feasibility

Algorithm 4: Solution to $(\mathcal{P}2)$

```

1: Invoke Alg. 3 to obtain  $\boldsymbol{\theta}^*$  and ranking  $\{\pi_i\}_{i=1}^{M_{\text{RIS}}}$ ;
2: Set EE = 0;
3: for  $J = 0$  to  $M_{\text{RIS}} - 1$  do
4:   Set  $\mathcal{A}(J) = \{\pi_{J+1}, \dots, \pi_{M_{\text{RIS}}}\}$ ;
5:   if  $(\mathcal{P}2(\mathcal{A}(J)))$  is infeasible then
6:     Break for;
7:   else
8:     Solve  $(\mathcal{P}2(\mathcal{A}(J)))$  and obtain the corresponding
       $\mathbf{F}^{\text{tmp}}$ ,  $\boldsymbol{\Theta}^{\text{tmp}}$  and  $\text{EE}^{\text{tmp}}$ ;
9:   end if
10:  if  $\text{EE}^{\text{tmp}} \geq \text{EE}$  then
11:     $\mathbf{F} = \mathbf{F}^{\text{tmp}}$ ,  $\boldsymbol{\Theta} = \boldsymbol{\Theta}^{\text{tmp}}$ ,  $\text{EE} = \text{EE}^{\text{tmp}}$ ,  $\mathcal{A} = \mathcal{A}^{\text{tmp}}$ ;
12:  end if
13: end for

```

and optimize its EE via Alg. 3 (if feasible). Lastly, we choose variables associated with the maximal EE as our final solution.

The overall approach for $(\mathcal{P}2)$ is summarized in Algorithm 4, where $(\mathcal{P}2(\mathcal{A}(J)))$ denotes the problem $(\mathcal{P}2)$ when the active set is given as $\mathcal{A}(J)$.

C. Computational Complexity Analysis

The complexity of Alg. 3 is dominated by solving the problem $(\mathcal{P}9)$ and $(\mathcal{P}10)$, which respectively needs $\mathcal{O}(K^{3.5}(M_{\text{AP}} + 1)^3 + K^{4.5}(M_{\text{AP}} + 1)M_{\text{AP}}^2)$ and $\mathcal{O}((K + N_{\text{RIS}})^{3.5} + (K + N_{\text{RIS}})^{2.5}N_{\text{RIS}}^2)$ operations. Thus, the complexity of handling $(\mathcal{P}8)$ can be expressed as $\mathcal{O}_3 = \mathcal{O}(T_2(K^{3.5}(M_{\text{AP}} + 1)^3 + K^{4.5}(M_{\text{AP}} + 1)M_{\text{AP}}^2 + (K + N_{\text{RIS}})^{3.5} + (K + N_{\text{RIS}})^{2.5}N_{\text{RIS}}^2))$, where T_2 represents the iteration times of tackling $(\mathcal{P}7)$. Moreover, Alg. 4 utilizes Alg. 3 and Alg. 5 both M_{RIS} times, whose complexity is given by $\mathcal{O}_4 = M_{\text{RIS}}(\mathcal{O}_3 + \mathcal{O}_5) + \mathcal{O}_3$.

V. FEASIBILITY CHARACTERIZATION

In this section, we will investigate the feasibility characterization of the problems $(\mathcal{P}4)$ and $(\mathcal{P}7)$.

A. Problem Formulation

Before going into details, we first clarify the significance of characterizing the feasibility of $(\mathcal{P}4)$ and $(\mathcal{P}7)$, both of which have identical constraints. For one thing, we need an initial feasible solution to solve $(\mathcal{P}4)$ and $(\mathcal{P}7)$ (refer to Alg. 1 and Alg. 3). For another, we must check the feasibility given a specific active set of sub-arrays (refer to step 5 of Alg. 2 and step 5 of Alg. 4).

The feasibility characterization problem of $(\mathcal{P}4)$ and $(\mathcal{P}7)$ is given as

$$(\mathcal{P}11) : \text{Find } (\mathbf{F}, \boldsymbol{\Theta}) \quad (34)$$

$$\text{s.t. } \sum_{k=1}^K \|\mathbf{f}_k\|_2^2 \leq P_{\text{AP,max}}, \quad (34a)$$

$$\tilde{P}_{\text{RIS}}(\mathbf{F}, \boldsymbol{\Theta}) \leq P_{\text{RIS,max}}, \quad (34b)$$

$$\tilde{R}_k(\mathbf{v}, \mathbf{w}, \mathbf{F}, \boldsymbol{\Theta}) \geq R_k, \quad k \in \mathcal{K}, \quad (34c)$$

$$\beta_n \leq \beta_{n,\text{max}}, \quad \theta_n \in [0, 2\pi), \quad n \in \mathcal{N}, \quad (34d)$$

The above problem is troublesome since its objective is missing. Now we consider another relevant problem as follows

$$(\mathcal{P}12) : \min_{\mathbf{F}, \boldsymbol{\Theta}, \kappa} \kappa \quad (35)$$

Algorithm 5: Solution to $(\mathcal{P}11)$

```

1: Randomly generate  $\mathbf{F}^{(0)}$ ,  $\boldsymbol{\Theta}^{(0)}$ ,  $\kappa^{(0)}$  and  $t = 0$ ;
2: repeat
3:   update  $\mathbf{v}^{(t+1)}$  by function (21);
4:   update  $\mathbf{w}^{(t+1)}$  by function (22);
5:   update  $(\mathbf{F}^{(t+1)}, \kappa^{(t+\frac{1}{2})})$  by solving  $(\mathcal{P}13)$ ;
6:   update  $(\boldsymbol{\Theta}^{(t+1)}, \kappa^{(t+1)})$  by solving  $(\mathcal{P}14)$ ;
7:    $t := t + 1$ ;
8: until convergence
9: if  $\kappa < 0$  then
10:   Obtain feasible  $(\mathbf{v}, \mathbf{w}, \mathbf{F}, \boldsymbol{\Theta})$  for  $(\mathcal{P}4)$  and  $(\mathcal{P}7)$ ;
11: else
12:   Claim infeasible;
13: end if

```

$$\text{s.t. } \sum_{k=1}^K \|\mathbf{f}_k\|_2^2 - P_{\text{AP,max}} \leq \kappa, \quad (35a)$$

$$\tilde{P}_{\text{RIS}}(\mathbf{F}, \boldsymbol{\Theta}) - P_{\text{RIS,max}} \leq \kappa, \quad (35b)$$

$$R_k - \tilde{R}_k(\mathbf{v}, \mathbf{w}, \mathbf{F}, \boldsymbol{\Theta}) \leq \kappa, \quad k \in \mathcal{K}, \quad (35c)$$

$$\beta_n \leq \beta_{n,\text{max}}, \quad \theta_n \in [0, 2\pi), \quad n \in \mathcal{N}. \quad (35d)$$

If the optimal solution $(\mathbf{F}^*, \boldsymbol{\Theta}^*, \kappa^*)$ to $(\mathcal{P}12)$ yields $\kappa^* \leq 0$, then $(\mathbf{F}^*, \boldsymbol{\Theta}^*)$ is actually a feasible solution to $(\mathcal{P}11)$. Otherwise, $(\mathcal{P}11)$ is infeasible. Therefore, we aim at solving the problem $(\mathcal{P}12)$. One advantage of $(\mathcal{P}12)$ is that it's always feasible (provided κ is chosen sufficiently large).

B. Proposed Algorithm

Next, we tackle the problem $(\mathcal{P}12)$, where we adopt the BCD approach.

1) Optimize auxiliary variable \mathbf{v}

The update of \mathbf{v} can still be obtained via (21).

2) Optimize auxiliary variable \mathbf{w}

The optimization of \mathbf{w} can still be obtained by (22) as before.

3) Optimize beamforming at the AP \mathbf{F}

The optimization problem for \mathbf{F} is given by

$$(\mathcal{P}13) : \min_{\mathbf{F}, \kappa} \kappa \quad (36)$$

$$\text{s.t. } \sum_{k=1}^K \|\mathbf{f}_k\|_2^2 - P_{\text{AP,max}} \leq \kappa, \quad (36a)$$

$$\tilde{P}_{\text{RIS}}(\mathbf{F}|\boldsymbol{\Theta}) - P_{\text{RIS,max}} \leq \kappa, \quad (36b)$$

$$R_k - \tilde{R}_k(\mathbf{F}|\mathbf{v}, \mathbf{w}, \boldsymbol{\Theta}) \leq \kappa, \quad k \in \mathcal{K}, \quad (36c)$$

which is a convex problem and can be numerically solved.

4) Optimize the RIS configuration $\boldsymbol{\Theta}$

For update of $\boldsymbol{\Theta}$, following similar arguments tackling $(\mathcal{P}6)$, $\boldsymbol{\Theta}$ can be optimized via solving the following problem

$$(\mathcal{P}14) : \min_{\boldsymbol{\Theta}, \kappa} \kappa \quad (37)$$

$$\text{s.t. } \boldsymbol{\theta}^T \mathbf{P} \boldsymbol{\theta}^* + g(\boldsymbol{\theta}|\boldsymbol{\theta}^{(t)}) L_{\text{RIS}} P_{\text{c,RIS}} - P_{\text{RIS,max}} \leq \kappa, \quad (37a)$$

$$\boldsymbol{\theta}^T \mathbf{Q}_k \boldsymbol{\theta}^* + 2\text{Re}\{\mathbf{q}_k^H \boldsymbol{\theta}^*\} + q_k - r_k \leq \kappa, \quad k \in \mathcal{K}, \quad (37b)$$

$$|\theta_n| \leq \beta_{n,\text{max}}, \quad n \in \mathcal{N}, \quad (37c)$$

where the notations follow the definition in (26). $(\mathcal{P}14)$ is convex and can be solved numerically.

The overall alternative optimization procedure is summarized in Alg. 5. If the obtained κ^* by Alg. 5 is no larger than zero,

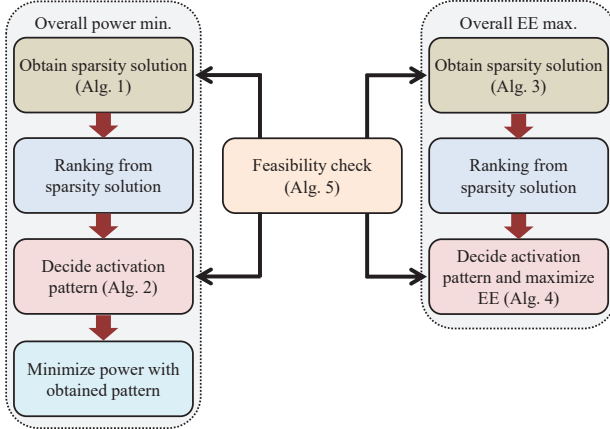


Fig. 3. Work flow of solving $(\mathcal{P}1)$ and $(\mathcal{P}2)$.

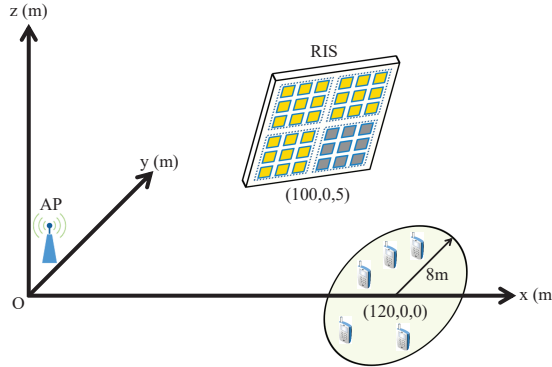


Fig. 4. Simulation scenario.

then a feasible solution to $(\mathcal{P}11)$ has actually been found. Note that when κ^* obtained by Alg. 5 is positive, it does not mean that $(\mathcal{P}11)$ is definitely infeasible. In fact, $(\mathcal{P}11)$ is non-convex and BCD algorithm generally doesn't guarantee converging to globally optimal solutions of non-convex problems. Therefore, theoretically, it is possible that the globally optimal $\kappa^{**} < 0$. However, since we cannot find the globally optimal solution, we have to claim that $(\mathcal{P}11)$ is infeasible. Notice that $(\mathcal{P}12)$ is also applicable for any specific active set $\mathcal{A} \subseteq \mathcal{M}$, which will be useful for Alg. 2 and Alg. 4 to check feasibility (in their step 5).

We also have the following theorem as elaborated above:

Theorem 3. *The solution iterates generated by Alg. 5 yield monotonically decreasing objective values of $(\mathcal{P}12)$.*

Proof. This can be proved following the arguments in Thm. 1 and Thm. 2. Hence, we omit it for space limitation. \square

Moreover, we present a flow chart in Fig. 3 summarizing the processes to attack power minimization and EE maximization.

C. Computational Complexity analysis

The complexity of solving $(\mathcal{P}13)$ and $(\mathcal{P}14)$ is $\mathcal{O}(K^{4.5}M_{AP}^3)$ and $\mathcal{O}((K + N_{RIS})^{1.5}N_{RIS}^3)$, respectively. Therefore, the total complexity of Alg. 5 is approximately

TABLE I: Simulation Parameters

Parameters	Values
Maximal transmit radio power of the AP $P_{AP,max}$	25dBm
Maximal power supply at the RIS $P_{RIS,max}$	1W
Dissipated power of the AP $P_{c,AP}$	2W
Dissipated power of each reflecting element $P_{c,RIS}$	2.5mW
Dissipated power of the users $P_{c,k}$, $k \in \mathcal{K}$	10dBm
Noise power at the RIS and users σ_{RIS}^2 , σ_k^2 , $k \in \mathcal{K}$	-80dBm
Number of reflecting elements N_{RIS}	300
Amplifying coefficients $\beta_{n,max}$, $n \in \mathcal{N}$	80
Inverse of the emission efficiency of the AP ξ_{AP}	1.2
Inverse of the emission efficiency of the RIS ξ_{RIS}	1.2

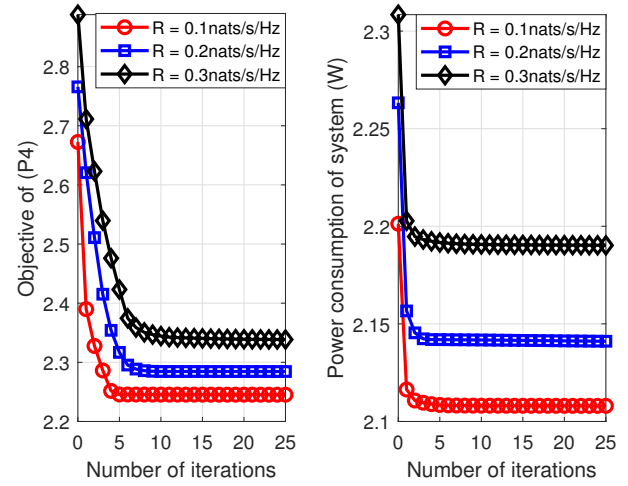


Fig. 5. Convergence of Alg. 1 and power minimization with obtained \mathcal{A} ($M_{RIS} = 15$).

given as $\mathcal{O}_5 = \mathcal{O}(T_3(K^{4.5}M_{AP}^3 + (K + N_{RIS})^{1.5}N_{RIS}^3))$ with T_3 denoted as the number of iterations to handle $(\mathcal{P}12)$.

VI. SIMULATION RESULTS

In this section, extensive numerical results will be presented to demonstrate the benefit of our proposed sub-array based RIS activation scheme and the effectiveness of our proposed algorithms. As shown in Fig. 4, we consider a system where an AP with $M_{AP} = 8$ antennas located at the origin serves $K = 5$ users which are randomly distributed within a circle with its center at $(120m, 0, 0)$ and radius of 8m. The active RIS is positioned at $(100m, 0, 5m)$. Unless otherwise specified, the system settings are given in Table I. Besides, the distance-dependent pathloss is modeled as $PL(d) = C_0(d/d_0)^{-\alpha}$, where $C_0 = -30$ dB is the pathloss at the reference $d_0 = 1$ m, d stands for the propagation distance and α represents the pathloss exponent. The AP-RIS channel \mathbf{G} is assumed to follow the line-of-sight (LoS) and its pathloss exponent is $\alpha_{AI} = 2.5$. Moreover, we suppose $\mathbf{h}_{r,k}$ and $\mathbf{h}_{d,k}$ follow Rayleigh fading distribution with the pathloss exponents of $\alpha_{IU} = 2.8$ and $\alpha_{AU} = 3.8$, respectively.

In the following, we will present the convergence of our proposed algorithms corresponding to their optimization problems.

A. Convergence

Firstly, Fig. 5 demonstrates the effectiveness of Alg. 1. The left part of Fig. 5 illustrates the convergence of Alg. 1 in solving

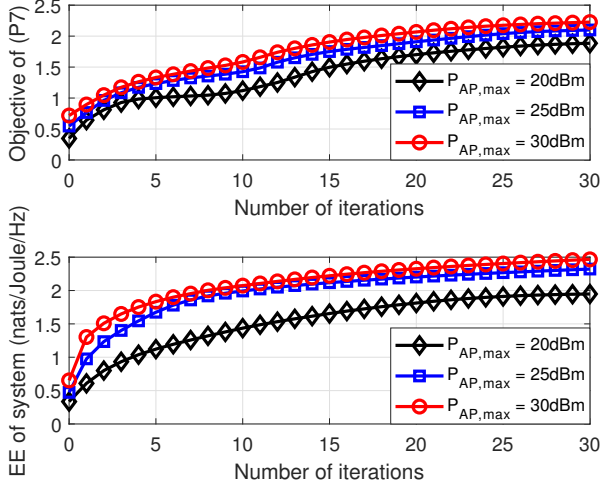


Fig. 6. Convergence of Alg. 3 and EE maximization with obtained \mathcal{A} ($M_{\text{RIS}} = 15$, $R_k = 0.1\text{nats/s/Hz}$, $k \in \mathcal{K}$).

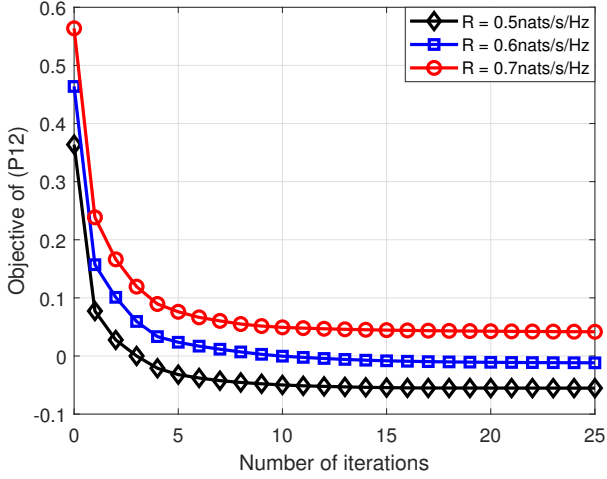


Fig. 7. Convergence of Alg. 5 ($M_{\text{RIS}} = 15$).

($\mathcal{P}4$). The right part of this figure plots Alg. 1's convergence when the activation pattern is finally determined. As can be seen, the objective value monotonically decreases and generally converges within 10 iterations.

Fig. 6 illustrates the convergence of Alg. 3. In the upper half of Fig. 6 presents the convergence performance when tackling ($\mathcal{P}7$). In the lower half of this figure shows Alg. 3's convergence with finally obtained \mathcal{A} . It can be observed that, the objective value monotonically increases and reaches convergence within about 30 iterations.

Besides, we examine the convergence of Alg. 5 for the feasibility characterization in Fig. 7. It can be seen that the algorithm generally converges within approximately 15 iterations. Besides, the optimal κ is monotonically increasing when the QoS requirements increase, which reflects that high QoS thresholds shrink the feasibility domain or even lead to infeasibility, as illustrated via the red curve in Fig. 7.

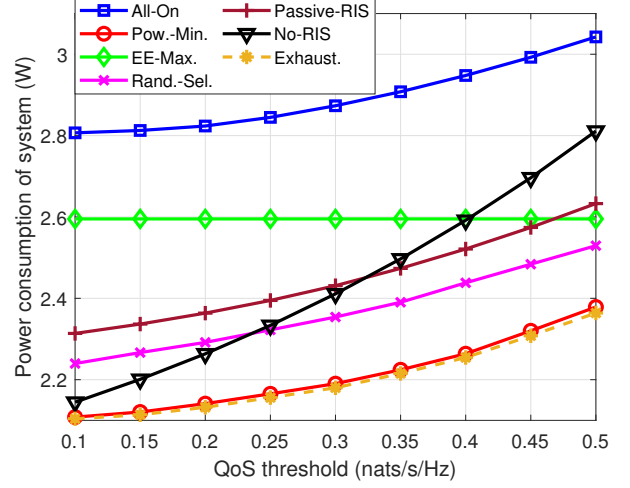


Fig. 8. The impact of QoS threshold on power consumption of the system ($M_{\text{RIS}} = 15$).

TABLE II: Avg. Num. of Activated Sub-arrays for Power Min.

QoS threshold [nats/s/Hz]	0.52	0.54	0.56	0.58	0.60
Exhaust.	1.04	1.40	2.08	3.60	7.28
Pow.-Min.	1.16	1.48	2.24	3.76	7.52
EE.-Max.	3.96	4.24	4.76	6.12	9.44
Rand.-Sel.	4.74	5.21	6.04	7.97	11.87

B. Experiments for Power Minimization

The impact of QoS threshold on power consumption of the system is investigated in Fig. 8. Besides our proposed algorithm, we also present other sub-array activation schemes for comparison, which include: i) All-On: all the sub-arrays are always switched-on, ii) EE-Max.: the power consumption associated with our proposed EE maximization solution (i.e. Alg. 4), iii) Rand.-Sel.: operate power minimization among 150 randomly selected sub-array activation patterns and calculate the average power, iv) Passive RIS: replace the active RIS by a passive one [5] with N_{RIS} elements, each of which consumes a little power (e.g. $P_{c,\text{RIS}} = 0.6\text{mW}$ [16]) and set $P_{\text{AP},\text{max}} := P_{\text{AP},\text{max}} + P_{\text{RIS},\text{max}} - N_{\text{RIS}}P_{c,\text{RIS}}$ for fairness, v): No-RIS: the active RIS is removed and set $P_{\text{AP},\text{max}} := P_{\text{AP},\text{max}} + P_{\text{RIS},\text{max}}$ for a fair comparison, vi): Exhaust.: minimize power among all the subsets \mathcal{A} and select the optima. Compared to the conventional “All-On” scheme, our sub-array based configuration has accomplished substantial power saving. Most importantly, our algorithm can achieve nearly identical performance with that obtained via the exhaustive search based solution, but with a much lower complexity.

We repeat the aforementioned various sub-array activation schemes under a number of random channel realizations and present the obtained average number of activated sub-arrays in Table II. As suggested by the table, our proposed algorithm can yield almost identical number of switched-on sub-arrays as that by exhaustive searching method. Note that the exhaustive search solution has a $2^{M_{\text{RIS}}}$ searching complexity, while ours is only of $\log(M_{\text{RIS}})$.

Fig. 9 plots the impact of the granularity of the sub-arrays on the power saving performance. In the experiment, the total

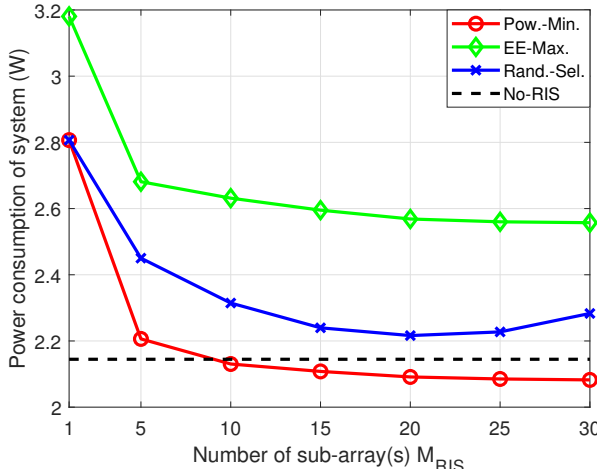


Fig. 9. The impact of number of sub-array(s) on power consumption of the system ($R_k = 0.1\text{nats/s/Hz}$, $k \in \mathcal{K}$).

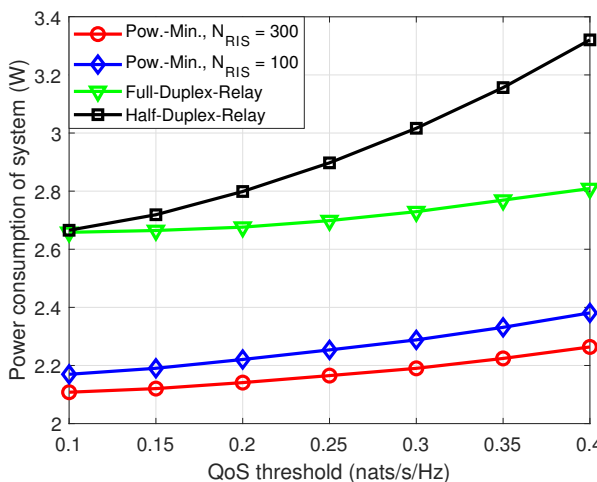


Fig. 10. Comparison of power consumption between sub-array based active RIS and HD-/FD-relays.

number of RIS reflecting elements is fixed at 300. We vary the size of sub-array (i.e. L_{RIS}) and test the activation scheme's performance. As suggested in Fig. 9, more power saving gain can be obtained when the RIS is partitioned into sub-arrays with smaller size. Intuitively, smaller sub-array leads to a more precise activation at the expense of a higher computational complexity. Note that for "Rand.-Sel." scheme, we always search 150 random activation patterns. When M_{RIS} gets large, the randomly selected 150 activation patterns covers only a small fraction of the whole pattern space. Therefore, "Rand.-Sel." performance degrades when M_{RIS} grows. Besides, when $M_{\text{RIS}} = 1$, our proposed sub-array structure boils down to the conventional "All-On" scheme and yields a large total power consumption, which is even larger than the "No-RIS" case. We need stress that this phenomenon does not contradict the results obtained in the existing literature, e.g., [5], since we consider the power consumption including the non-transmit part, which is generally ignored in other works on power minimization.

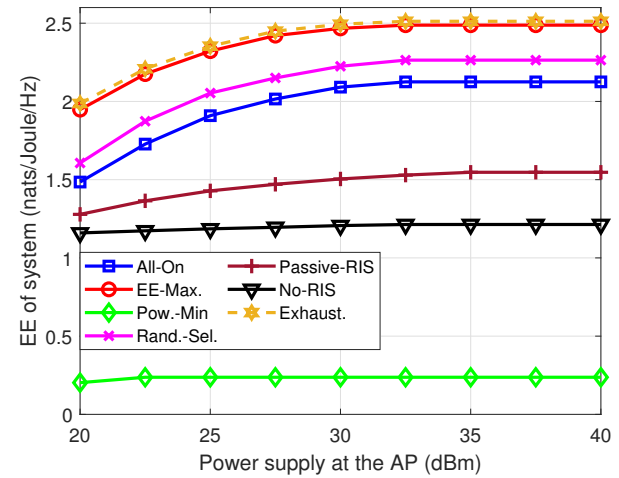


Fig. 11. The impact of power supply at the AP on the EE of the system ($M_{\text{RIS}} = 15$, $R_k = 0.1\text{nats/s/Hz}$, $k \in \mathcal{K}$).

TABLE III: Avg. Num. of Activated Sub-arrays for EE Max.

$P_{\text{AP},\text{max}}$ [dBm]	20	25	30	35	40
Exhaust.	6.24	3.16	2.20	1.04	1.04
EE-Max.	6.44	3.28	2.24	1.08	1.08
Pow.-Min.	4.08	1.00	1.00	1.00	1.00
Rand.-Sel.	9.77	6.64	5.33	4.15	4.15

In Fig. 10, we compare the performance of power consumption among half-duplex (HD)-relay, full-duplex (FD)-relay and our proposed sub-array based active RIS, where the size of sub-array (i.e. L_{RIS}) is fixed at 20. The same system settings reported in Table I are adopted for relay scenarios, where both relays are assumed to have identical number of antennas as that of the AP and the dissipated power at both relays are given by $P_{\text{c,relay}} = 600\text{mW}$ [46]. It can be observed from Fig. 10 that the sub-array based active RIS significantly outperforms both relays. The reason lies in that the beamforming gain led by the active RIS is higher since its number of "reflecting" elements is larger than the number of antennas of relays. Besides, with a larger N_{RIS} , we can achieve more power reduction due to more sub-arrays and more flexibility.

C. Experiments for EE Maximization

Fig. 11 illustrates the impact of power supply at the AP on the EE of the system, where the curve labelled as "Pow.-Min." represents the EE associated with the power minimization solution (i.e. Alg. 2). As presented in Fig. 11, when $P_{\text{AP},\text{max}}$ is inadequate, EE monotonically improves along with the power supply increasing. Comparatively, when the power supply is sufficient, EE will tend to become constant. This is because, at this time, more transmit radio power can only bring marginal information rate improvement. Besides, our proposed algorithm can achieve nearly identical performance as that of exhaustive search based solution.

Similar to the experiment above, the average number of activated sub-arrays by four activation schemes for EE maximization is reported in Table III. It can be observed that the numbers of turned-on sub-arrays obtained from "EE-Max." and

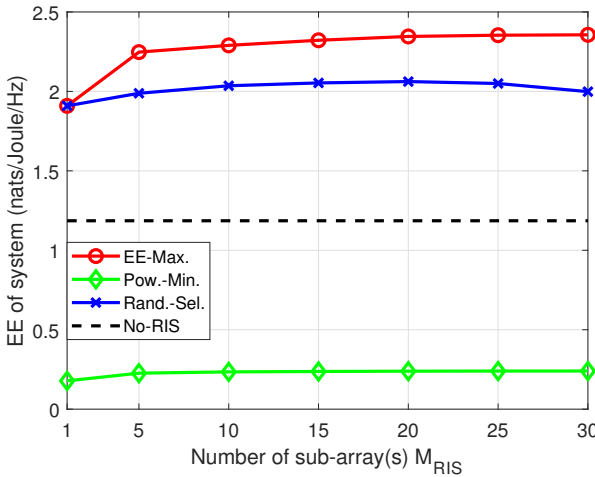


Fig. 12. The impact of number of sub-array(s) on the EE of the system ($R_k = 0.1\text{nats/s/Hz}$, $k \in \mathcal{K}$).

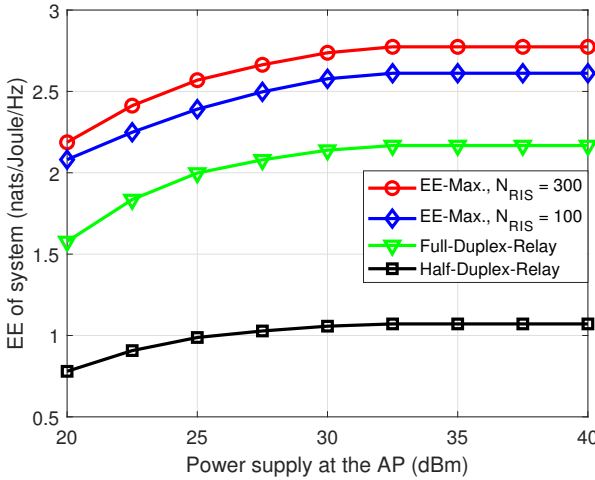


Fig. 13. Comparison of EE between sub-array based active RIS and HD/FD-relays.

“Exhaust.” nearly coincide, but ours only has a M_{RIS} searching complexity.

The impact of granularity of sub-arrays on the EE performance is plotted in Fig. 12. The total number of reflecting elements is still fixed at 300. As can be seen, smaller sub-array size yields a higher EE since finer activation of reflecting elements can be realized, but with a higher complexity.

Fig. 13 plots the comparison of EE between HD/FD-relays and our proposed active RIS architecture. As suggested by this figure, via wisely selecting the beamforming of the sub-arrays with advantageous channel conditions, the system’s EE can be improved significantly.

Lastly, in Table IV, we present the running time of our proposed solutions and exhaustive searching methods for power and EE optimization. As suggested by this table, our proposed algorithms can significantly reduce the complexity while yielding nearly the identical performances as the exhaustive searching methods. Note that we perform these simulations on

TABLE IV: Comparison of Running Time (in Sec.) of Proposed Solutions and Exhaustive Search ($M_{\text{RIS}} = 10$)

Optimization Problem	Setting	Prop.	Exhaustive Search
Pow.-Min.	$R = 0.1\text{nats/s/Hz}$	75.17	2.643×10^4
	$R = 0.6\text{nats/s/Hz}$	102.8	3.154×10^4
EE-Max.	$P_{\text{AP},\text{max}} = 20\text{dBm}$	594.2	5.511×10^4
	$P_{\text{AP},\text{max}} = 30\text{dBm}$	671.9	5.535×10^4

our personal desktop computer, whose computational capability is believed to be much lower than that equipped in the AP.

VII. CONCLUSION

In this paper, a novel sub-array based active RIS structure was proposed to reduce non-negligible energy consumed by the active components in the reflecting elements. Based on this novel sub-array based implementation, we successfully developed efficient solutions to solve the power minimization and EE maximization problem via jointly designing the RIS activation patterns, beamformings of the AP and the RIS. Numerical results verified that our proposed solutions can achieve nearly identical exhaustive search based solutions and significantly improve the power and the EE performances by up to 25% and 31%, respectively.

APPENDIX

A. Proof of Theorem 1

Proof. Assume a feasible solution $(\mathbf{v}^{(t)}, \mathbf{w}^{(t)}, \mathbf{F}^{(t)}, \Theta^{(t)})$ to $(\mathcal{P}4)$ has been obtained. Then, in the next iteration, $\mathbf{v}^{(t+1)} = \arg \max_{\mathbf{v}} \tilde{R}_k(\mathbf{v}|\mathbf{w}^{(t)}, \mathbf{F}^{(t)}, \Theta^{(t)})$, $k \in \mathcal{K}$, and $\tilde{R}_k(\mathbf{v}^{(t+1)}, \mathbf{w}^{(t)}, \mathbf{F}^{(t)}, \Theta^{(t)}) \geq \tilde{R}_k(\mathbf{v}^{(t)}, \mathbf{w}^{(t)}, \mathbf{F}^{(t)}, \Theta^{(t)}) \geq R_k$, $k \in \mathcal{K}$, which indicates that $(\mathbf{v}^{(t+1)}, \mathbf{w}^{(t)}, \mathbf{F}^{(t)}, \Theta^{(t)})$ is feasible as well. Similarly, $(\mathbf{v}^{(t+1)}, \mathbf{w}^{(t+1)}, \mathbf{F}^{(t)}, \Theta^{(t)})$ remains feasible, which implies that the feasible domain of $(\mathcal{P}5)$ is not empty and we can obtain the updated $(\mathbf{v}^{(t+1)}, \mathbf{w}^{(t+1)}, \mathbf{F}^{(t+1)}, \Theta^{(t)})$, which is naturally feasible to $(\mathcal{P}4)$. Note that (20b) and (25a) have identical value at the point of $\Theta^{(t)}$, which immediately implies that $(\mathbf{v}^{(t+1)}, \mathbf{w}^{(t+1)}, \mathbf{F}^{(t+1)}, \Theta^{(t)})$ is also feasible to $(\mathcal{P}6)$. By solving $(\mathcal{P}6)$, we obtain $(\mathbf{v}^{(t+1)}, \mathbf{w}^{(t+1)}, \mathbf{F}^{(t+1)}, \Theta^{(t+1)})$ which is feasible to $(\mathcal{P}6)$. Utilizing the fact that (25a) is upper bound of (20b), we conclude that $(\mathbf{v}^{(t+1)}, \mathbf{w}^{(t+1)}, \mathbf{F}^{(t+1)}, \Theta^{(t+1)})$ is indeed also feasible to $(\mathcal{P}4)$. Thus we have proved that the solution iterates remain feasible.

Denote $P(\mathbf{v}, \mathbf{w}, \mathbf{F}, \Theta)$ as the objective value of $(\mathcal{P}4)$ and $\tilde{P}(\mathbf{v}, \mathbf{w}, \mathbf{F}, \Theta|\Theta^{(t)})$ as the convex upper bound of $P(\mathbf{v}, \mathbf{w}, \mathbf{F}, \Theta)$ after MM. Then, we have

$$\begin{aligned}
 & P(\mathbf{v}^{(t+1)}, \mathbf{w}^{(t+1)}, \mathbf{F}^{(t+1)}, \Theta^{(t+1)}) \\
 & \stackrel{(a)}{\leq} \tilde{P}(\mathbf{v}^{(t+1)}, \mathbf{w}^{(t+1)}, \mathbf{F}^{(t+1)}, \Theta^{(t+1)}|\Theta^{(t)}) \\
 & \stackrel{(b)}{\leq} \tilde{P}(\mathbf{v}^{(t+1)}, \mathbf{w}^{(t+1)}, \mathbf{F}^{(t+1)}, \Theta^{(t)}|\Theta^{(t)}) \\
 & \stackrel{(c)}{=} P(\mathbf{v}^{(t+1)}, \mathbf{w}^{(t+1)}, \mathbf{F}^{(t+1)}, \Theta^{(t)}) \stackrel{(d)}{\leq} P(\mathbf{v}^{(t+1)}, \mathbf{w}^{(t+1)}, \mathbf{F}^{(t)}, \Theta^{(t)}) \\
 & \stackrel{(e)}{=} P(\mathbf{v}^{(t+1)}, \mathbf{w}^{(t)}, \mathbf{F}^{(t)}, \Theta^{(t)}) \stackrel{(f)}{=} P(\mathbf{v}^{(t)}, \mathbf{w}^{(t)}, \mathbf{F}^{(t)}, \Theta^{(t)}),
 \end{aligned} \tag{38}$$

where (a) holds due to the fact that $\tilde{P}(\mathbf{v}, \mathbf{w}, \mathbf{F}, \Theta|\Theta^{(t)})$ is an upper bound of $P(\mathbf{v}, \mathbf{w}, \mathbf{F}, \Theta)$, (c) follows since $\tilde{P}(\mathbf{v}, \mathbf{w}, \mathbf{F}, \Theta|\Theta^{(t)})$ and $P(\mathbf{v}, \mathbf{w}, \mathbf{F}, \Theta)$ coincide at the point of

$\Theta^{(t)}$. (b) and (d) hold since optimizations lower the objective and the equalities (e) and (f) stand because v and w have no effect on objective value of (20), which proves the monotonically decreasing of the objective. Since the objective of $(\mathcal{P}4)$ is obviously bounded from below (larger than 0), the objective sequence converges. \square

B. Proof of Theorem 2

Proof. The feasible domains of (v, w, F, Θ) associated with $(\mathcal{P}7)$ and $(\mathcal{P}8)$ are evidently identical. Suppose that we have obtained a feasible solution $(v^{(t)}, w^{(t)}, x^{(t)}, y^{(t)}, F^{(t)}, \Theta^{(t)})$ to $(\mathcal{P}8)$. Since the updates of v and w only increase $\tilde{R}_k(v, w, F, \Theta)$ in (29a), $(v^{(t+1)}, w^{(t+1)}, x^{(t)}, y^{(t)}, F^{(t)}, \Theta^{(t)})$ remains feasible, which implies that $(\mathcal{P}9)$ has non-empty feasible domain. Via solving $(\mathcal{P}9)$, $(v^{(t+1)}, w^{(t+1)}, x^{(t+\frac{1}{2})}, y^{(t+\frac{1}{2})}, F^{(t+1)}, \Theta^{(t)})$ is obtained and it's naturally a feasible solution to $(\mathcal{P}9)$. Since the constraint function in (32e) is a lower-bound of that in (29e) (refer to (31)), $(v^{(t+1)}, w^{(t+1)}, x^{(t+\frac{1}{2})}, y^{(t+\frac{1}{2})}, F^{(t+1)}, \Theta^{(t)})$ is also feasible to $(\mathcal{P}8)$, which can be set as a feasible point of $(\mathcal{P}10)$. Following the similar discussions above, we can conclude that $(v^{(t+1)}, w^{(t+1)}, x^{(t+1)}, y^{(t+1)}, F^{(t+1)}, \Theta^{(t+1)})$ after solving $(\mathcal{P}10)$ is also feasible to $(\mathcal{P}8)$, so is $(\mathcal{P}7)$.

Define $\text{EE}(v, w, F, \Theta) \triangleq \frac{\sum_{k=1}^K \tilde{R}_k(v, w, F, \Theta)}{\tilde{P}_{\text{total}}(F, \Theta)} = \frac{\sum_{k=1}^K x_k^2(v, w, F, \Theta)}{y(F, \Theta)}$ $\triangleq \tilde{\text{EE}}(x, y)$, where $x_k(v, w, F, \Theta) \triangleq \sqrt{\tilde{R}_k(v, w, F, \Theta)}$, $k \in \mathcal{K}$, and $y(F, \Theta) \triangleq \tilde{P}_{\text{total}}(F, \Theta)$, and $\tilde{P}_u(F, \Theta | \Theta^{(t)})$ denotes the left hand side of (33b). Then

$$\begin{aligned} & \text{EE}(v^{(t+1)}, w^{(t+1)}, F^{(t+1)}, \Theta^{(t+1)}) \stackrel{(a)}{=} \tilde{\text{EE}}(x^{(t+1)}, y^{(t+1)}) \\ & \stackrel{(b)}{\geq} \tilde{\text{EE}}(x^{(t+\frac{1}{2})}, y^{(t+\frac{1}{2})}) + \sum_{k=1}^K \left(\frac{2x_k^{(t+\frac{1}{2})}}{y^{(t+\frac{1}{2})}} (x_k^{(t+1)} - x_k^{(t+\frac{1}{2})}) \right. \\ & \quad \left. - \frac{(x_k^{(t+\frac{1}{2})})^2}{(y^{(t+\frac{1}{2})})^2} (\tilde{P}_{\text{total}}(F^{(t+1)}, \Theta^{(t+1)}) - y^{(t+\frac{1}{2})}) \right) \\ & \stackrel{(c)}{\geq} \tilde{\text{EE}}(x^{(t+\frac{1}{2})}, y^{(t+\frac{1}{2})}) + \sum_{k=1}^K \left(\frac{2x_k^{(t+\frac{1}{2})}}{y^{(t+\frac{1}{2})}} (x_k^{(t+1)} - x_k^{(t+\frac{1}{2})}) \right. \\ & \quad \left. - \frac{(x_k^{(t+\frac{1}{2})})^2}{(y^{(t+\frac{1}{2})})^2} (\tilde{P}_u(F^{(t+1)}, \Theta^{(t+1)} | \Theta^{(t)}) - y^{(t+\frac{1}{2})}) \right) \\ & \stackrel{(d)}{=} \tilde{\text{EE}}(x^{(t+\frac{1}{2})}, y^{(t+\frac{1}{2})}) + \sum_{k=1}^K \left(\frac{2x_k^{(t+\frac{1}{2})}}{y^{(t+\frac{1}{2})}} (x_k^{(t+1)} - x_k^{(t+\frac{1}{2})}) \right. \\ & \quad \left. - \frac{(x_k^{(t+\frac{1}{2})})^2}{(y^{(t+\frac{1}{2})})^2} (y^{(t+1)} - y^{(t+\frac{1}{2})}) \right) \\ & \stackrel{(e)}{\geq} \tilde{\text{EE}}(x^{(t+\frac{1}{2})}, y^{(t+\frac{1}{2})}) + \sum_{k=1}^K \left(\frac{2x_k^{(t+\frac{1}{2})}}{y^{(t+\frac{1}{2})}} (x_k^{(t+\frac{1}{2})} - x_k^{(t+\frac{1}{2})}) \right. \\ & \quad \left. - \frac{(x_k^{(t+\frac{1}{2})})^2}{(y^{(t+\frac{1}{2})})^2} (y^{(t+\frac{1}{2})} - y^{(t+\frac{1}{2})}) \right) = \tilde{\text{EE}}(x^{(t+\frac{1}{2})}, y^{(t+\frac{1}{2})}) \\ & = \text{EE}(v^{(t+1)}, w^{(t+1)}, F^{(t+1)}, \Theta^{(t)}) \\ & \stackrel{(f)}{\geq} \text{EE}(v^{(t+1)}, w^{(t+1)}, F^{(t)}, \Theta^{(t)}) \stackrel{(g)}{\geq} \text{EE}(v^{(t)}, w^{(t)}, F^{(t)}, \Theta^{(t)}), \end{aligned} \quad (39)$$

where $x_k^{(t+1)} \triangleq x_k(v^{(t+1)}, w^{(t+1)}, F^{(t+1)}, \Theta^{(t+1)})$, $x_k^{(t+\frac{1}{2})} \triangleq x_k(v^{(t+1)}, w^{(t+1)}, F^{(t+1)}, \Theta^{(t)})$, $k \in \mathcal{K}$ and $y^{(t+\frac{1}{2})} \triangleq \tilde{P}_{\text{total}}(F^{(t+1)}, \Theta^{(t)})$. The equality (a) follows from the above definitions. Referring to (30), we have the inequality (b),

and (c) stands since $\tilde{P}_u(F, \Theta | \Theta^{(t)})$ is an upper bound of $\tilde{P}_{\text{total}}(F, \Theta)$. When $(\mathcal{P}10)$ gets solved, one key observation is that the constraints (33a) and (33b) achieve equalities, i.e., $x_k^{(t+1)} = x_k^{(t+\frac{1}{2})}$, $k \in \mathcal{K}$, $y^{(t+1)} = \tilde{P}_u(F^{(t+1)}, \Theta^{(t+1)} | \Theta^{(t)})$, since the objective (33) is linear in (x, y) , which implies the equality (d) with the settings $x_k^{(t+\frac{1}{2})} = x_k^{(t+\frac{1}{2})}$, $k \in \mathcal{K}$ and $y^{(t+\frac{1}{2})} = y^{(t+\frac{1}{2})}$, and (e) holds since the update of Θ by solving $(\mathcal{P}10)$ increases the objective. Following the similar procedures (b)-(e), we can obtain (f). Lastly, (g) is concluded from the fact that the updates of v and w only increase the numerator of the objective (28), which means that the value of (28) monotonically increases. Obviously, the objective value of $(\mathcal{P}7)$ is bounded from above. Therefore, its objective sequence converges. \square

REFERENCES

- [1] H. Tataria, M. Shafi, A. F. Molisch, M. Dohler, H. Sjöland, and F. Tufvesson, "6G wireless systems: Vision, requirements, challenges, insights, and opportunities," in *Proceedings of the IEEE*, vol. 109, no. 7, pp. 1166–1199, Jul. 2021.
- [2] C. Pan and *et al.*, "Reconfigurable intelligent surfaces for 6G systems: Principles, applications, and research directions," *IEEE Commun. Mag.*, vol. 59, no. 6, pp. 14–20, Jun. 2021.
- [3] Q. Wu, X. Guan, and R. Zhang, "Intelligent reflecting surface-aided wireless energy and information transmission: An overview," in *Proceedings of the IEEE*, vol. 110, no. 1, pp. 150–170, Jan. 2022.
- [4] C. Pan, H. Ren, K. Wang, W. Xu, M. Elkashlan, A. Nallanathan, and L. Hanzo, "Multicell MIMO communications relying on intelligent reflecting surfaces," *IEEE Trans. Wireless Commun.*, vol. 19, no. 8, pp. 5218–5233, Aug. 2020.
- [5] Q. Wu and R. Zhang, "Intelligent reflecting surface enhanced wireless network via joint active and passive beamforming," *IEEE Trans. Wireless Commun.*, vol. 18, no. 11, pp. 5394–5409, Nov. 2019.
- [6] C. Huang, A. Zappone, G. C. Alexandropoulos, M. Debbah, and C. Yuen, "Reconfigurable intelligent surfaces for energy efficiency in wireless communication," *IEEE Trans. Wireless Commun.*, vol. 18, no. 8, pp. 4157–4170, Aug. 2019.
- [7] Q. Wu and R. Zhang, "Joint active and passive beamforming optimization for intelligent reflecting surface assisted SWIPT under QoS constraints," *IEEE J. Sel. Areas Commun.*, vol. 38, no. 8, pp. 1735–1748, Aug. 2020.
- [8] Y. Yang, B. Zheng, S. Zhang, and R. Zhang, "Intelligent reflecting surface meets OFDM: Protocol design and rate maximization," *IEEE Trans. Commun.*, vol. 68, no. 7, pp. 4522–4535, Jul. 2020.
- [9] J. Zhu, Y. Huang, J. Wang, K. Navaie, and Z. Ding, "Power efficient IRS-assisted NOMA," *IEEE Trans. Commun.*, vol. 69, no. 2, pp. 900–913, Feb. 2021.
- [10] Z. Chu, Z. Zhu, F. Zhou, M. Zhang, and N. A.-Dahir, "Intelligent reflecting surface assisted wireless powered sensor networks for internet of things," *IEEE Trans. Commun.*, vol. 69, no. 7, pp. 4877–4899, Jul. 2021.
- [11] Q. Wu, S. Zhang, B. Zheng, C. You, and R. Zhang, "Intelligent reflecting surface-aided wireless communications: A tutorial," *IEEE Trans. Commun.*, vol. 69, no. 5, pp. 3313–3351, May 2021.
- [12] E. Björnson, Ö. Özdogan, and E. G. Larsson, "Intelligent reflecting surface versus decode-and-forward: How large surfaces are needed to beat relaying?" *IEEE Wireless Commun. Lett.*, vol. 9, no. 2, pp. 244–248, Feb. 2020.
- [13] Z. Zhang, L. Dai, X. Chen, C. Liu, F. Yang, R. Schober, and H. V. Poor, "Active RIS vs. passive RIS: Which will prevail in 6G?" Mar. 2022. [Online]. Available: <https://arxiv.org/abs/2103.15154v5>
- [14] E. Basar and H. V. Poor, "Present and future of reconfigurable intelligent surface-empowered communications," *IEEE Signal Process. Mag.*, vol. 38, no. 6, pp. 146–152, Nov. 2021.
- [15] C. You and R. Zhang, "Wireless communication aided by intelligent reflecting surface: Active or passive?" *IEEE Wireless Commun. Lett.*, vol. 10, no. 12, pp. 2659–2663, Dec. 2021.
- [16] R. Long, Y.-C. Liang, Y. Pei, and E. G. Larsson, "Active reconfigurable intelligent surface-aided wireless communications," *IEEE Trans. Wireless Commun.*, vol. 20, no. 8, pp. 4962–4975, Aug. 2021.
- [17] Z. Yigit, E. Basar, M. Wen, and I. Altunbas, "Hybrid reflection modulation," Nov. 2021. [Online]. Available: <https://arxiv.org/abs/2111.08355v1>

- [18] K. Liu, Z. Zhang, L. Dai, S. Xu, and F. Yang, "Active reconfigurable intelligent surface: Fully-connected or sub-connected?" *IEEE Commun. Lett.*, vol. 26, no. 1, pp. 167–171, Jan. 2022.
- [19] R. A. Tasci, F. Kılinc, E. Basar, and G. C. Alexandropoulos, "A new RIS architecture with a single power amplifier: Energy efficiency and error performance analysis," *IEEE Access*, vol. 10, pp. 44804–44815, 2022.
- [20] Y. Gao, C. Yang, Z. Xiong, J. Zhao, Y. Xiao, and D. Niyato, "Reflection resource management for intelligent reflecting surface aided wireless networks," *IEEE Trans. Commun.*, vol. 69, no. 10, pp. 6971–6986, Oct. 2021.
- [21] Q. Wang, Z. Gao, Y. Xu, and H. Xie, "Energy-efficient optimization for IRS-assisted wireless-powered communication networks," in *Proc. IEEE Veh. Technol. Conf. (VTC)*, Helsinki, Finland, Apr. 2021.
- [22] Z. Yang, M. Chen, W. Saad, W. Xu, M. S.-Bahaei, H. V. Poor, and S. Cui, "Energy-efficient wireless communications with distributed reconfigurable intelligent surfaces" *IEEE Trans. Wireless Commun.*, vol. 21, no. 1, pp. 665–679, Jan. 2022.
- [23] Huawei AP1050DN-S access point datasheet, Huawei. [Online]. Available: <https://e.huawei.com/en/material/networking/wlan/2b4fd557e436423e99059250ccaa9281>, 2017.
- [24] A. Kaushik, J. Thompson, E. Vlachos, C. Tsinos, and S. Chatzinotas, "Dynamic RF chain selection for energy efficient and low complexity hybrid beamforming in millimeter wave MIMO systems," *IEEE Trans. Green Commun. Netw.*, vol. 3, no. 4, pp. 886–900, Dec. 2019.
- [25] F. Yang, J.-B. Wang, M. Cheng, J.-Y. Wang, M. Lin, and J. Cheng, "A partially dynamic subarrays structure for wideband mmWave MIMO systems," *IEEE Trans. Commun.*, vol. 68, no. 12, pp. 7578–7592, Dec. 2020.
- [26] G. M. Gadiel, N. T. Nguyen, and K. Lee, "Dynamic unequally sub-connected hybrid beamforming architecture for massive MIMO systems," *IEEE Trans. Veh. Technol.*, vol. 70, no. 4, pp. 3469–3478, Apr. 2021.
- [27] H. Li, M. Li, and Q. Liu, "Hybrid beamforming with dynamic subarrays and low-resolution PSs for mmWave MU-MISO systems," *IEEE Trans. Commun.*, vol. 68, no. 1, pp. 602–614, Jan. 2020.
- [28] J.-B. Wang, X. Wang, F. Yang, H. Zhang, M. Lin, and J. Wang, "Intelligent reflecting surface aided millimeter wave communication using subarray-connected structure," *IEEE Trans. Veh. Technol.*, vol. 71, no. 5, pp. 5581–5586, May 2022.
- [29] N. T. Nguyen, K. Lee, and H. Dai, "Hybrid beamforming and adaptive RF chain activation for uplink cell-free millimeter-wave massive MIMO systems," *IEEE Trans. Veh. Technol.*, vol. 71, no. 8, pp. 8739–8755, Aug. 2022.
- [30] S. Wan, H. Zhu, K. Kang, and H. Qian, "On the performance of fully-connected and sub-connected hybrid beamforming system," *IEEE Trans. Veh. Technol.*, vol. 70, no. 10, pp. 11078–11082, Oct. 2021.
- [31] W. Huang, Z. Lu, Y. Huang, and L. Yang, "Hybrid precoding for single carrier wideband multi-subarray millimeter wave systems," *IEEE Wireless Commun. Lett.*, vol. 8, no. 2, pp. 484–487, Apr. 2019.
- [32] X. Zhao, T. Lin, Y. Zhu, and J. Zhang, "Partially-connected hybrid beamforming for spectral efficiency maximization via a weighted MMSE equivalence," *IEEE Trans. Wireless Commun.*, vol. 20, no. 12, pp. 8218–8232, Dec. 2021.
- [33] Q. Zhu, M. Li, R. Liu, Y. Liu, and Q. Liu, "Joint beamforming designs for active reconfigurable intelligent surface: A sub-connected array architecture," *IEEE Trans. Commun.*, vol. 70, no. 11, pp. 7628–7643, Nov. 2022.
- [34] S. Zhang, S. Zhang, F. Gao, J. Ma, and O. A. Dobre, "Deep learning optimized sparse antenna activation for reconfigurable intelligent surface assisted communication," *IEEE Trans. Commun.*, vol. 69, no. 10, pp. 6691–6705, Oct. 2021.
- [35] X. Xu, S. Zhang, F. Gao, and J. Wang, "Sparse bayesian learning based channel extrapolation for RIS assisted MIMO-OFDM," *IEEE Trans. Commun.*, vol. 70, no. 8, pp. 5498–5513, Aug. 2022.
- [36] Z. Wan, Z. Gao, F. Gao, M. D. Renzo, and M.-S. Alouini, "Terahertz massive MIMO with holographic reconfigurable intelligent surface," *IEEE Trans. Commun.*, vol. 69, no. 7, pp. 4732–4750, Jul. 2021.
- [37] M. Wu, Z. Gao, Y. Huang, Z. Xiao, D. W. K. Ng, and Z. Zhang, "Deep learning-based rate-splitting multiple access for reconfigurable intelligent surface-aided tera-hertz massive MIMO," *IEEE J. Sel. Areas Commun.*, to appear.
- [38] E. Björnson, J. Hoydis, and L. Sanguinetti, "Massive MIMO networks: Spectral, energy, and hardware efficiency," *Foundat. Trends Signal Process.*, vol. 11, no. 3–4, pp. 154–655, 2017.
- [39] M. Tao, E. Chen, H. Zhou, and W. Yu, "Content-centric sparse multicast beamforming for cache-enabled cloud RAN," *IEEE Trans. Wireless Commun.*, vol. 15, no. 9, pp. 6118–6131, Sep. 2016.
- [40] Y. Sun, P. Babu, and D. P. Palomar, "Majorization-minimization algorithms in signal processing, communications, and machine learning," *IEEE Trans. Signal Process.*, vol. 65, no. 3, pp. 794–816, Feb. 2017.
- [41] Q. Shi, M. Razavizayyan, Z.-Q. Luo, and C. He, "An iteratively weighted MMSE approach to distributed sum-utility maximization for a MIMO interfering broadcast channel," *IEEE Trans. Signal Process.*, vol. 59, no. 9, pp. 4331–4340, Sep. 2011.
- [42] A. Wiesel, Y. C. Eldar, and S. Shamai, "Linear precoding via conic optimization for fixed MIMO receivers," *IEEE Trans. Signal Process.*, vol. 54, no. 1, pp. 161–176, Jan. 2006.
- [43] M. Grant and S. Boyd, "CVX: MATLAB software for disciplined convex programming," 2016. [Online]. Available: <http://cvxr.com/cvx>
- [44] Y. Shi, J. Zhang, and K. B. Letaief, "Group sparse beamforming for green cloud-RAN," *IEEE Trans. Wireless Commun.*, vol. 13, no. 5, pp. 2809–2823, May 2014.
- [45] W. Dinkelbach, "On nonlinear fractional programming," *Manage. Sci.*, vol. 13, no. 7, pp. 492–498, Mar. 1967.
- [46] SR600EX, High Power Wireless-N 600mW Pro Smart Repeater, Amped Wireless. [Online]. Available: <https://ampedwireless.com/family/sr600ex.html>



Yanze Zhu received the B.S. degree in electronics information engineering from the Dalian University of Technology, Dalian, China, in 2021, where he is currently pursuing the M.S. degree with the School of Information and Communication Engineering. His current research interests include intelligent reflecting surfaces, channel estimation, and extremely large antenna array systems.



Yang Liu received the Ph.D. degree in Electrical Engineering from Lehigh University, PA, USA, in 2016. Before that he received the B.E. and M.E. degrees in Electrical Engineering from Beijing University of Posts and Telecommunications (BUPT), Beijing, China, in 2007 and 2010, respectively. In 2016, He worked as a senior engineer in Marvell Semiconductor Ltd., Santa Clara, CA, USA. From 2016 to 2019, he worked as a research engineer in Huawei Technologies Co., Ltd., Shanghai, China. From Nov. 2019 to April 2020, he worked as a postdoctoral research fellow in Nanyang Technological University (NTU), Singapore. He is currently an associate professor in the School of Information and Communication Engineering, Dalian University of Technology, Dalian, China. His research interests include error correction coding, multi-antenna wireless communication systems, intelligent reflective surface and wireless sensor networks.



Ming Li (S'05-M'11-SM'17) received the M.S. and Ph.D. degrees in electrical engineering from the State University of New York at Buffalo (SUNY-Buffalo), Buffalo, in 2005 and 2010, respectively. From Jan. 2011 to Aug. 2013, he was a Post-Doctoral Research Associate with the Signals, Communications, and Networking Research Group, Department of Electrical Engineering, SUNY-Buffalo. From Aug. 2013 to June 2014, Dr. Li joined Qualcomm Technologies Inc. as a Senior Engineer. Since June 2014, he has been with the School of Information and Communication Engineering, Dalian University of Technology, Dalian, China, where he is presently an Associate Professor. His current research interests are in the general areas of communication theory and signal processing with applications to intelligent reflecting surface, mmWave communications, secure wireless communications, cognitive radios and networks.



Qingqing Wu (S'13-M'16-SM'21) received the B.Eng. and the Ph.D. degrees in Electronic Engineering from South China University of Technology and Shanghai Jiao Tong University (SJTU) in 2012 and 2016, respectively. From 2016 to 2020, he was a Research Fellow in the Department of Electrical and Computer Engineering at National University of Singapore. He is currently an Associate Professor with Shanghai Jiao Tong University. His current research interest includes intelligent reflecting surface (IRS), unmanned aerial vehicle (UAV) communications, and MIMO transceiver design. He has coauthored more than 100 IEEE journal papers with 29 ESI highly cited papers and 9 ESI hot papers, which have received more than 19,000 Google citations. He was listed as the Clarivate ESI Highly Cited Researcher in 2022 and 2021, the Most Influential Scholar Award in AI-2000 by Aminer in 2021 and World's Top 2% Scientist by Stanford University in 2020 and 2021.

He was the recipient of the IEEE Communications Society Asia Pacific Best Young Researcher Award and Outstanding Paper Award in 2022, the IEEE Communications Society Young Author Best Paper Award in 2021, the Outstanding Ph.D. Thesis Award of China Institute of Communications in 2017, the Outstanding Ph.D. Thesis Funding in SJTU in 2016, the IEEE ICCC Best Paper Award in 2021, and IEEE WCSP Best Paper Award in 2015. He was the Exemplary Editor of IEEE Communications Letters in 2019 and the Exemplary Reviewer of several IEEE journals. He serves as an Associate Editor for IEEE Transactions on Communications, IEEE Communications Letters, IEEE Wireless Communications Letters, IEEE Open Journal of Communications Society (OJ-COMS), and IEEE Open Journal of Vehicular Technology (OJVT). He is the Lead Guest Editor for IEEE Journal on Selected Areas in Communications on "UAV Communications in 5G and Beyond Networks", and the Guest Editor for IEEE OJVT on "6G Intelligent Communications" and IEEE OJ-COMS on "Reconfigurable Intelligent Surface-Based Communications for 6G Wireless Networks". He is the workshop co-chair for IEEE ICC 2019-2022 workshop on "Integrating UAVs into 5G and Beyond", and the workshop co-chair for IEEE GLOBECOM 2020 and ICC 2021 workshop on "Reconfigurable Intelligent Surfaces for Wireless Communication for Beyond 5G". He serves as the Workshops and Symposia Officer of Reconfigurable Intelligent Surfaces Emerging Technology Initiative and Research Blog Officer of Aerial Communications Emerging Technology Initiative. He is the IEEE Communications Society Young Professional Chair in Asia Pacific Region.



Qingjiang Shi received his Ph.D. degree in electronic engineering from Shanghai Jiao Tong University (SJTU), Shanghai, China, in 2011. From September 2009 to September 2010, he visited Prof. Z.-Q. (Tom) Luo's research group at the University of Minnesota, Twin Cities. In 2011, he worked as a Research Scientist at Bell Labs China. From 2012, He was with the School of Information and Science Technology at Zhejiang Sci-Tech University. From Feb. 2016 to Mar. 2017, he worked as a research fellow at Iowa State University, USA. From Mar. 2018, he is currently a full professor with the School of Software Engineering at Tongji University. He is also with the Shenzhen Research Institute of Big Data. His interests lie in algorithm design and analysis with applications in machine learning, signal processing and wireless networks. So far he has published more than 70 IEEE journals and filed about 30 national patents.

Dr. Shi was an Associate Editor for the IEEE TRANSACTIONS ON SIGNAL PROCESSING. He was the recipient of the Huawei Outstanding Technical Achievement Award in 2021, the Huawei Technical Cooperation Achievement Transformation Award (2nd Prize) in 2022, the Golden Medal at the 46th International Exhibition of Inventions of Geneva in 2018, the First Prize of Science and Technology Award from China Institute of Communications in 2017, the National Excellent Doctoral Dissertation Nomination Award in 2013, the Shanghai Excellent Doctorial Dissertation Award in 2012, and the Best Paper Award from the IEEE PIMRC'09 conference.